REPORT DOCUMENTATION PAGE

Form Approved
OMB No. 0704-0188

1. AGENCY USE ONLY (Leave blank)	2. REPORT DATE	3. REPORT TYPE AND DATES COVERED
	March 1997	Final (Nov 1993 - Oct 1996)

4. TITLE AND SUBTITLE

Experimental Study of Factors Controlling Instability of Frictional Materials

5. FUNDING NUMBERS

AFOSR
Grant No. F49620-94-1-0032

6. AUTHOR(S)

Poul V. Lade

7. PERFORMING ORGANIZATION NAME(S) AND ADDRESS(ES)

The Johns Hopkins University
Department of Civil Engineering
Baltimore, Maryland 21218

AFOSR-TR-97
0163

9. SPONSORING / MONITORING AGENCY NAME(S) AND ADDRESS(ES)

AFOSR NA
Bolling AFB, DC 20332-6448

10. SPONSORING / MONITORING AGENCY REPORT NUMBER

94-1-0032

11. SUPPLEMENTARY NOTES

19970602 035

12a. DISTRIBUTION / AVAILABILITY STATEMENT

Unlimited

12b. DISTRIBUTION CODE

DISTRIBUTION STATEMENT A
Approved for public release
Distribution Unlimited

13. ABSTRACT (Maximum 200 words)

The objectives of the experimental investigations being reported here were to further study the factors that control the stability and instability of frictional materials. The study is divided into two parts: (1) Conditions for Instability, in which a coarse sand was tested at a total of three void ratios to study effects of density as well as additional aspects of instability of granular materials. These experiments were conducted in high pressure triaxial equipment (cell pressures up to 70 MPa). (2) Creep in Sand, in which a fundamental study of creep and relaxation of granular materials was performed, because time-dependent behavior has considerable influence on the stability of granular materials. The sand employed in the experiments had weak, easily crushed grains, which typically exhibit considerable creep. The experiments were performed under drained conditions in order to maintain a constant stress state. Various stress states were used to study whether the plastic potential can be used for prediction of the relative magnitudes of the inelastic creep strain increments, and to examine the effect of creep on the outward movement of the plastic yield surface. This in turn will control the conditions for instability.

14. SUBJECT TERMS	15. NUMBER OF PAGES
Granular Materials; high pressures; instability; drained creep; stress-strain behavior; pore pressures	74
	16. PRICE CODE

17. SECURITY CLASSIFICATION OF REPORT	18. SECURITY CLASSIFICATION OF THIS PAGE	19. SECURITY CLASSIFICATION OF ABSTRACT	20. LIMITATION OF ABSTRACT
Unclassified	Unclassified	Unclassified	UL

FINAL TECHNICAL REPORT

Grant No.: F49620-94-1-0032

Project Title:

Experimental Study of Factors Controlling Instability of Frictional Materials

Principal Investigator:

Poul V. Lade
Department of Civil Engineering
The Johns Hopkins University
3400 N. Charles Street
Baltimore, Maryland 21218-2686

March 1997

Table of Contents

Experimental Study of Factors Controlling Instability of Frictional Materials

by

Poul V. Lade

Introduction

Materials exhibiting nonassociated flow should according to stability postulates by Drucker and by Hill become unstable when exposed to certain stress paths inside the failure surface. Results of previously performed series of triaxial compression tests designed to expose the type of behavior displayed by granular materials form the basis for the objectives of the further studies supported by this grant. Stability and instability conditions for materials with nonassociated flow have previously been derived on the basis of the experimental results.

The objectives of the experimental investigations being reported here were to further study the factors that control the stability and instability of frictional materials. The study is divided into two parts: (1) Conditions for Instability, in which a coarse sand was tested at a total of three void ratios to study effects of density as well as additional aspects of instability of granular materials. These experiments were conducted in high pressure triaxial equipment (cell pressures up to 70 MPa). (2) Creep in Sand, in which a fundamental study of creep and relaxation of granular materials was performed, because time-dependent behavior has considerable influence on the stability of granular materials. The sand employed in the experiments had weak, easily crushed grains, which typically exhibit considerable creep. The experiments were performed under drained conditions in order to maintain a constant stress state. Various stress states were used to study whether the plastic potential can be used for prediction of the relative magnitudes of the inelastic creep strain increments, and to examine the effect of creep on the outward movement of the plastic yield surface. This in turn will control the conditions for instability.

The report takes the form of an executive summary with two major sections addressing the two central issues in the project. Section no. 1 is a paper which contains the essence of the major theme of the first part of the research, while section no. 2 is a paper on the experimental techniques and findings of the second part of the research study. The two parts of the study are briefly summarized below:

Effects of Initial Density on Soil Instability at High Pressures

A complete experimental study has been performed to investigate the effects of initial relative density on instability and the general framework of behavior of granular materials at high pressure. The bulk of the experimental program was centered on triaxial compression and

extension testing in both drained and undrained conditions over a confining pressure range between 0.25 and 60 MPa. In addition to thoroughly examining the deformation characteristics of Cambria sand, particular attention was directed to the area of membrane penetration, soil creep inside and outside the instability region, particle crushing, and behavior during isotropic and one-dimensional compression.

Results of undrained triaxial compression and extension tests were used to determine the instability characteristics of Cambria sand. The conditions under which a specimen exhibits unstable behavior was confirmed by performing a series of specialized instability tests. It appears that initiation of instability depends on the relationship between the shape of the yield surface and the effective stress path followed. The instability lines in compression and in extension vary slightly with density, but are otherwise straight lines through the stress origin.

Experimental Study of Drained Creep of Sand

The initial phases of this study consisted of developing triaxial equipment with steady pressures as well as mechanical devices (free of zero shift) for measuring deformations in the specimens. Two measuring systems were devised and employed to monitor the time-dependent deformations. One system consisted of conventional dial gages and volume change devices. The other system utilized a telescope mounted with micrometer screws to measure accurately to four pins stuck into the specimen to measure both vertical and horizontal deformations away from the (lubricated) ends of the triaxial specimen. It was found that the two systems measured essentially the same deformations with equal accuracy, and they therefore lend support to their mutual reliability.

Experiments were performed under drained conditions and include various stress paths within a range of confining pressures from 25 to 785 kPa. Time-dependent behavior was studied, including creep, relaxation, and one-dimensional compression performed with different stress magnitudes.

Other Studies

Several other major topics were studied under the auspices of this research project, and papers have been published, accepted for publication, or have been submitted for publication, as indicated in the lists of Journal Publications, Book Chapter, Conference Publications, and Recently Submitted Manuscripts. These papers were all published or prepared within the period of performance, all topics are related to the central themes, and they have been supported to some extent (small or large) by the funding provided for this research project. All publications contain appropriate acknowledgment to support from AFOSR.

Personnel Supported or Associated with Research Project:

Faculty: Lade, Poul V.

Postdoc: Yamamuro, Jerry A.

Graduate Students: Liu, C.-T. (Ted)
Bopp, Paul A.
Wang, Qiong

Undergraduate Students: Liggio, Carl D.
Leung, Alice
Borduin, Wayne

Ph.D. - Dissertations:

Chi-Tseng (Ted) Liu: "Experimental Study of Creep Behavior of Granular Materials," University of California, Los Angeles, June 1994.

Paul Andrew Bopp: "The Effect of Initial Relative density on Instability and behavior of Granular materials at High Pressure," University of California, Los Angeles, December 1994.

Journal Publications:

Lade, P.V., Bopp, P.A., and Peters, J.F., "Instability of dilating sand", *Mechanics of Materials,* Elsevier, Vol. 16, 1993, pp. 249-264.

Lade, P.V., "Initiation of static instability in the submarine Nerlerk berm", *Canadian Geotechnical Journal*, Vol. 30, No.5, December 1993, pp. 895-904.

Lade, P.V., "Creep Effects on Static and Cyclic Instability of Granular Soils", *Journal of Geotechnical Engineering*, ASCE, Vol. 120, No. 2, February, 1994, pp.404-419.

Lade, P.V., "Instability and Liquefaction of Granular Materials", *Computers and Geotechnics*, Vol. 16, 1994, pp. 123-151.

Yamamuro, J.A., and Lade, P.V., "Strain Localization in Extension Tests on Granular Materials," *Journal of Engineering Mechanics*, ASCE, Vol. 121, No. 7, July, 1995, pp.828-836.

Yamamuro, J.A. and Lade, P.V., "Drained Sand Behavior in Axisymmetric Tests at High Pressures," *Journal of Geotechnical Engineering*, ASCE, Vol. 122, No. 2, 1996, pp.109-119.

Lade, P.V. and Yamamuro, J.A., "Undrained Sand Behavior in Axisymmetric Tests at High Pressures," *Journal of Geotechnical Engineering*, ASCE, Vol. 122, No. 2, 1996, pp.120-129.

Yamamuro, J.A., Bopp, P.A., and Lade, P.V., "One-Dimensional Compression of Sands at High Pressures," *Journal of Geotechnical Engineering*, ASCE, Vol. 122, No. 2, 1996, pp.147-154.

Lade, P.V., Yamamuro, J.A., and Bopp, P.A., "Significance of Particle Crushing in Granular Materials," *Journal of Geotechnical Engineering*, ASCE, Vol. 122, 1996, pp.309-316.

Lade, P.V., Yamamuro, J.A., and Skyers, B.D., "Effects of Shear Band Formation in Triaxial Extension Tests," *Geotechnical Testing Journal*, GTJODJ, Vol. 19, No. 4, December 1996, pp.398-410.

Lade, P.V. and de Boer, R., "The concept of effective stress for soil, concrete, and rock," *Geotechnique*, Vol. 47, No. 1, 1997, pp. 61-78.

Yamamuro, J.A. and Lade, P.V., "Instability of Granular Materials at High Pressures," *Soils and Foundations*, Japanese Geotechnical Society, Vol. 37, No. 1, 1997 (accepted).

Bopp, P.A., and Lade, P.V., "Effects of Initial Density on Soil Instability at High Pressures," *Journal of Geotechnical and Geoenvironmental Engineering*, ASCE, Vol. 123, No. 7, 1997 (accepted).

Bopp, P.A., and Lade, P.V., "Membrane Penetration in Granular Materials," *Geotechnical Testing Journal*, ASTM, GTJODJ, Vol. 20, No. 3, September 1997 (accepted).

Lade, P.V., Yamamuro, J.A., and Bopp, P.A., "Influence of Time Effects on Instability of Granular Materials," *Computers and Geotechnics*, Elsevier, (accepted).

Book Chapter

Lade, P.V. "Influence of Creep on Static and Cyclic Instability of Granular Materials," Chapter 21 in *Modern Approaches to Plasticity*, edited by D. Kolymbas, Elsevier Science Publishers B.V., 1993, pp. 385-409.

Conference Publications

Lade, P. V., "Instability analysis for tailings slopes," *Proceedings of the 13th International Conference on Soil Mechanics and Foundation Engineering*, New Delhi, India, January 1994, pp. 1649-1652.

Lade, P.V., "Instability of sand in the prefailure hardening regime", *Proceedings of the International Symposium on Pre-Failure Deformation Characteristics of Geomaterials*, Sapporo, Japan, September 1994, Vol. 2, 1995, pp. 837-854.

Lade, P.V., Yamamuro, J.A., and Skyers, B.D., "Effects of strain localization in triaxial extension tests," *Proceedings of the Fifth International Symposium on Numerical Models in Geomechanics - NUMOG V*, Davos, Switzerland, edited by G.N. Pande and S.Pietruszczak, September 1995, pp. 187-192.

Yamamuro, J.A. and Lade, P.V., "Behavior and modeling of static liquefaction of silty sands," *Proceedings of the Sixth International Symposium on Numerical Models in Geomechanics - NUMOG VI*, Montreal, Canada, edited by G.N. Pande and S.Pietruszczak, July 1997 (accepted).

Yamamuro, J.A. and Lade, P.V., "Prediction of instability conditions for sand," *Proceedings of the 14th International Conference on Soil Mechanics and Foundation Engineering*, Hamburg, Germany, September 1997 (accepted).

Recently Submitted Manuscripts

Lade, P.V., Liggio, C.D., and Yamamuro, J.A., "Effects of non-plastic fines on density and compressibility of sand," *Geotechnical Testing Journal*, ASTM.

Yamamuro, J.A. and Lade, P.V., "Static liquefaction of very loose sands," *Canadian Geotechnical Journal.*

Lade, P.V. and Yamamuro, J.A., "Effects of non-plastic fines on static liquefaction of sands," *Canadian Geotechnical Journal.*

Lade, P.V. and Liu, C.-T., "Experimental Study of Drained Creep Behavior of Sand," *Journal of Engineering Mechanics*, ASCE.

Interactions:

Lade, Poul V., "Instability of Sand in the Prefailure Hardening Regime," Invited Keynote Lecture presented at the International Symposium on Pre-Failure Deformation Characteristics of Geomaterials - Measurement and Application (IS-Hokkaido '94), Sapporo, Japan, September 12-14, 1994.

Lade, Poul V. "The Concept of Effective Stress for Soil, Concrete, and Rock," Presented at the Department of Applied Mechanics and Engineering Science, University of California at San Diego, La Jolla, California, October 10, 1994.

Lade, Poul V. "Single and Double Hardening Plasticity Models for Frictional Materials - A Comparison," Invited lecture presented at The Fifth International Symposium on Plasticity and Its Current Applications: Plasticity '95: Dynamic Plasticity and Structural Behaviors, held at Sakai, Osaka, Japan, July 17-21, 1995.

Lade, Poul V. "Effects of Strain Localization in Triaxial Extension Tests," Invited Feature Lecture presented at NUMOG V, held in Davos, Switzerland, Sept. 6-9, 1995.

Lade, Poul V. "Experimental Study of Factors Controlling Instability of Frictional Materials," Presented at Particulate Mechanics Contractor/Grantee Meeting, Wright Laboratory, Tyndall AFB, Florida, September 22-23, 1995.

Lade, Poul V. "Modeling Time Effects and Instability of Granular Materials," presented at the Workshop on Sediment Geoacoustical and Geotechnical Constitutive Modeling, held at University of Rhode Island, Narrgansett, Rhode Island, November 13-14, 1995 (invited).

Lade, Poul V. "Instability and Liquefaction of Granular Materials," presented at University of Illinois, Urbana-Champaign, December 4, 1995 (invited).

Lade, Poul V. "Influence of Time Effects on Instability of Granular Materials," presented at the ASME Mechanics of Materials Conference, held at The Johns Hopkins University, June 12-14, 1996.

EFFECTS OF INITIAL DENSITY ON SOIL INSTABILITY AT HIGH PRESSURES

By Paul A. Bopp[1] and Poul V. Lade[2], Members, ASCE

ABSTRACT

A high-pressure triaxial compression and extension testing apparatus was utilized to investigate the effect of initial relative density on soil instability. Stress paths from a series of undrained tests, at confining pressures from 8 to 60 MPa, were evaluated to determine the location of the potential instability region. Results indicate initial relative density has a small effect on the slope of the instability line, with the slope of the line decreasing as initial density is reduced. In addition, the conditions under which a specimen exhibits unstable behavior were confirmed by performing a series of specialized instability tests. It was found that initiation of unstable behavior depends on the relationship between the shape of the yield surface and the effective stress path followed.

KEYWORDS

Compression, creep, extension, granular materials, high-pressure, instability, relative density, sands, triaxial test, undrained test

---

[1] Principal Geotechnical Engineer, Silverado Constructors, Irvine, Califomia 92614.

[2] Professor, Department of Civil Engineering, The Johns Hopkins University, Baltimore, Maryland 21218.

INTRODUCTION

Instability of granular materials has been an important topic in geotecnical engineering since the phenomenon of liquefaction was discovered. Historically, most research on instability has been performed at relatively low confining pressures, where loose sands compress and dense sands dilate during shear (Casagrande 1940; Lee and Seed 1967). It is important to note that the volume change behavior of a material directly relates to the question of stability. Generally, materials that dilate exhibit stable behavior until the failure surface has been reached, whereas materials that compress may become unstable inside the failure surface (Lade et al. 1987, 1988). The unique aspect of testing at high pressures is that the dilative nature of dense soils decreases with increasing confining pressure until only compressive behavior is observed during shear. This provides the necessary conditions under which even very dense soils can become unstable. Thus, testing at high pressures makes available a range of initial densities which will experience volumetric compression and affords the opportunity to evaluate the effect of initial relative density on the instability phenomenon of granular materials.

EXPERIMENTAL OBSERVATIONS OF INSTABILITY CONDITIONS

In the study presented herein instability is taken to be the inability of a soil to sustain or carry a given load, which includes the ability to sustain small perturbations in the loads. it should be noted that instability and failure are two different behavior aspects of soils which exhibit nonassociated flow. Although both may lead to catastrophic events, they are not synonymous. Simply stated, a failure surface does not go through each point at which

instability is produced. In fact, granular materials can exhibit unstable behavior in a large region inside the failure surface. This is explained in further detail below.

The state of stress at which instability can occur corresponds to the top of the current yield surface as shown schematically on the p'- q diagram in Fig. 1. Beyond this top point the soil can deform plastically under decreasing stresses. The top of the undrained effective stress path corresponding to $(\sigma_1 - \sigma_3)_{max}$ occurs slightly after but very close to the top of the yield surface. Accordingly, a line connecting the tops of a series of effective stress paths, from undrained tests on compressive soil, provides the lower limit of the region of potential instability. Experiments show that this line is straight and since it goes through the top points of the yield surfaces, which evolve from the origin, the instability line also intersects the stress origin (Lade 1993). In order for a granular material to become unstable, the state of stress must be located on or above the instability line and undrained conditions must be imposed. If the soil remains drained, it will remain stable, even in the region of potential instability.

Fig. 2 schematically shows the bottom of the wedge shaped instability region. The bottom is located where the undrained stress path becomes horizontal and does not increase to an ultimate state. Below this limit exists a narrow zone known as the temporary instability region. In this zone the soil first experiences compressive behavior and then dilatant behavior which stabilizes the soil and increases the capability to carry larger deviator stresses prior to reaching failure. The change in load carrying capability occurs at the phase transformation line (Ishihara et al. 1975) or the characteristic line (Loung, 1982). Below the lower limit of the temporary instability zone, the tendency for dilation dominates the soil

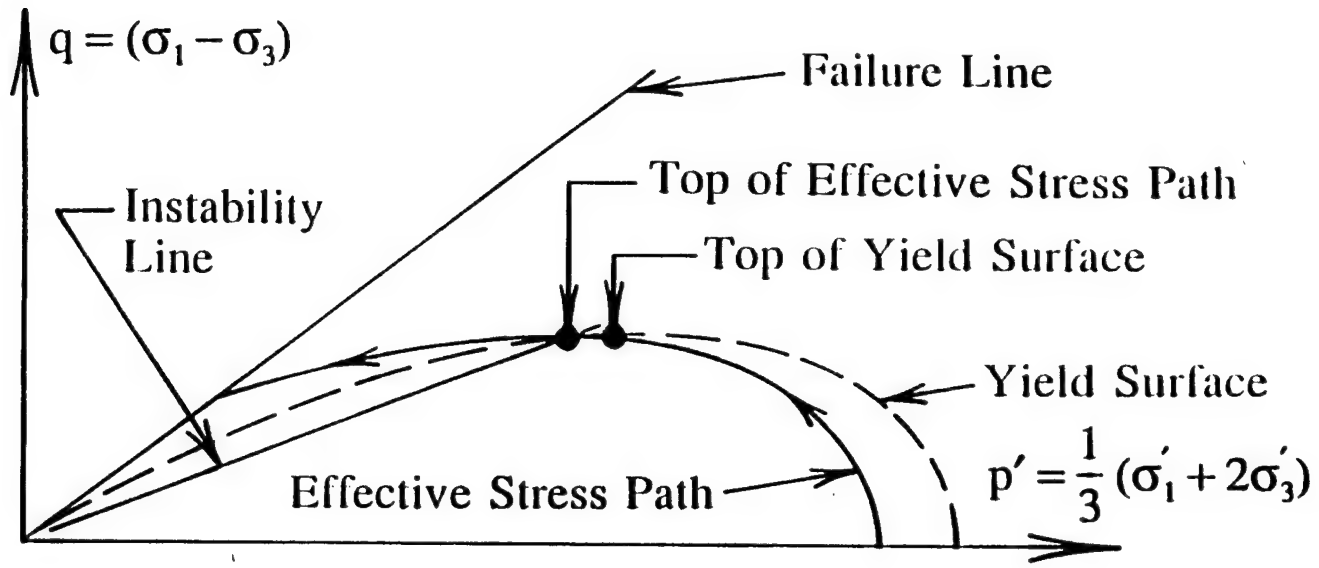

Fig. 1. Schematic diagram of location of instability line determined from consolidated-undrained test on loose sand.

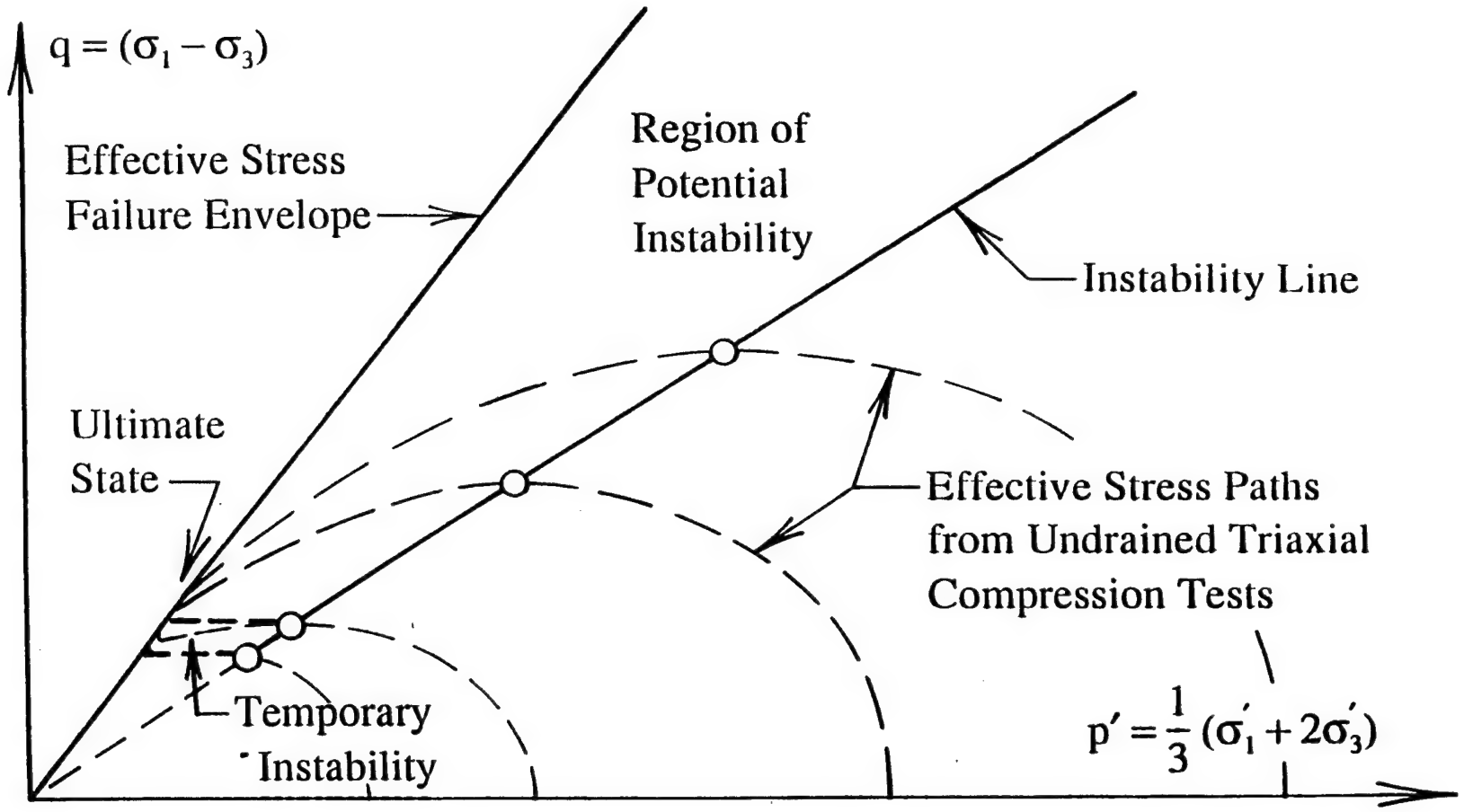

Fig. 2. Schematic diagram of location of instability line in $p' - q$ diagram.

behavior and a decrease in deviator stress is not observed under undrained conditions. The soil therefore exhibits only stable behavior within this region.

CHARACTERISTICS AND PREPARATION OF TEST SPECIMEN

In the experimental study, the granular material tested was Cambria sand. This coarse, uniform sand consists of sub-angular to well rounded grains with diameters between 0.83 and 2.00 millimeters. The maximum void ratio is 0.792, the minimum void ratio is 0.503, and the specific gravity is 2.69. The detrital composition of the Cambria sand is highly variable consisting mostly of quartz, with sedimentary, metamorphic and volcanic lithic grains also in abundance. In addition, minor amounts of feldspar, mica, dense accessory minerals and calcite are present.

Specimens tested in triaxial compression were cylindrical in shape and averaged approximately 7.1 centimeters in diameter and 17.8 centimeters in height, for a height-to-diameter ratio of 2.5. Triaxial extension specimens were also cylindrical in shape with equal height and diameter of 8.9 centimeters for a height-to-diameter ratio of 1.0.

The specimens were prepared by dry pluviation of the sand from a height of 18 centimeters for samples with initial relative density of 60% and zero height for initial relative density of 30%. Lubricated ends were employed in all tests to help enforce uniform strains. Following preparation, the specimens were saturated utilizing the $C0_2$-method as described by Lade and Duncan (1973). In addition, a back pressure of 0.52 MPa was applied to ensure the specimen had a high degree of saturation.

EXPERIMENTAL STUDY ON INSTABILITY

The zone of potential instability for the Cambria sand with initial relative density of 30% and 60% was determined by performing undrained compression and extension tests. Results of these tests are plotted on the Cambridge p'- q diagrams shown on Fig. 3. As can be seem, the instability line connects the top points of the effective stress paths from a series of undrained tests with progressively increasing initial confining pressures.

Only one compression specimen, tested at a confining pressure of 8 MPa and with initial relative density of 60%, plotted within the temporary instability region. The effective stress path followed by this test was nearly horizontal after the instability line was reached. The deviator stress increased only slightly to a maximum value just before intersecting the effective stress failure line. Therefore, the line representing the bottom of the instability region is drawn slightly above the near horizontal stress path of the 8.0 MPa test. All tests performed in both compression and extension with an initial relative density of 30%, and the remaining tests with initial relative density of 60%, exhibited general compressive behavior throughout and reached a maximum deviator stress value at the instability line. Consequently, the lower limit of the instability region for the compression tests with D_r = 30% must be below that of the D_r = 60% samples and for sufficiently loose sand it may reach the stress origin (Lade 1993). The exact location of the line could not be established, because undrained tests with initial confining pressures below 8 MPa were not performed due to adverse membrane penetration effects.

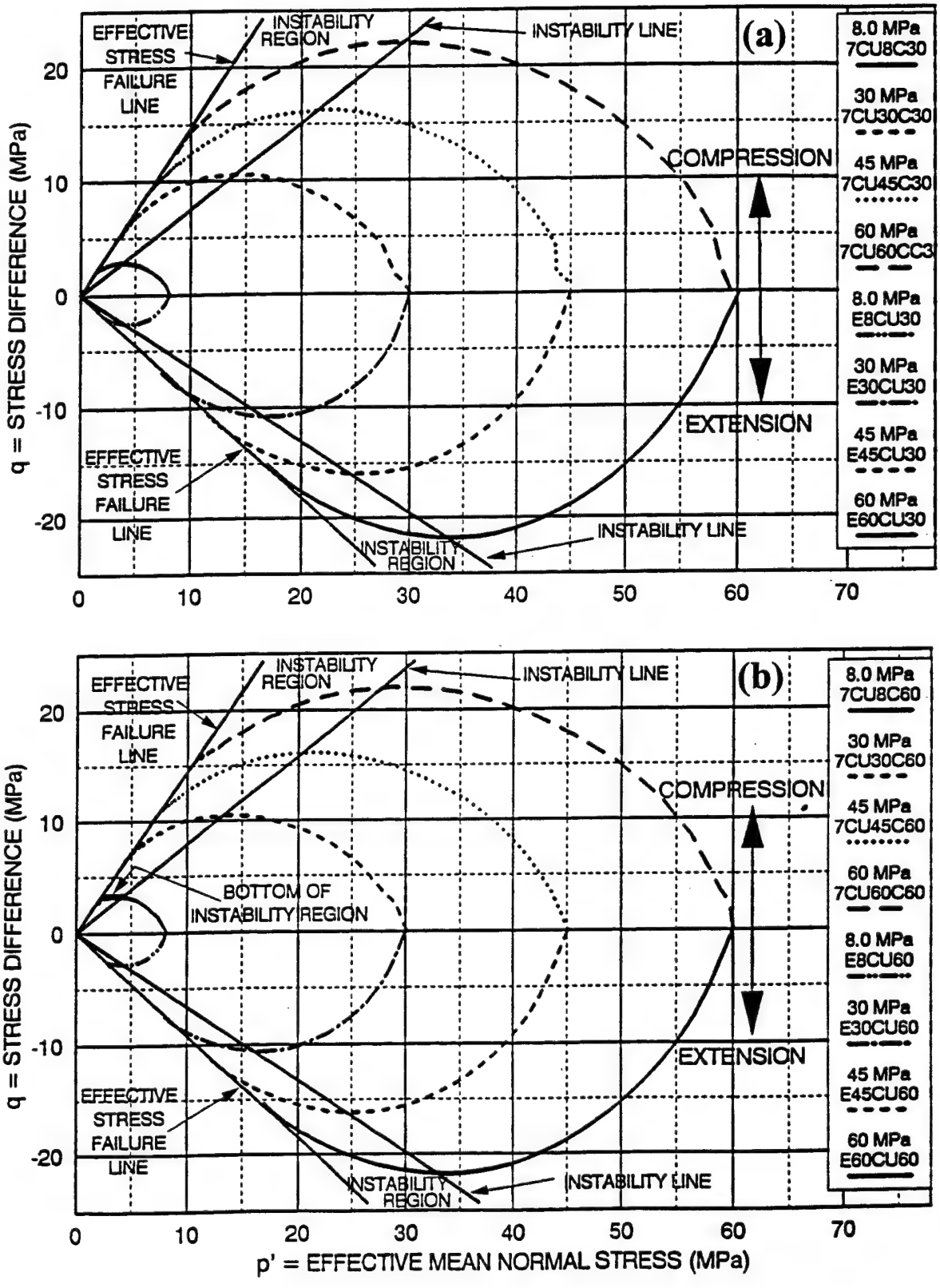

Fig. 3. Instability lines and failure lines determined from consolidated-undrained triaxial compression and extension tests on Cambria sand with initial relative densities of (a) 30%, and (b) 60%.

EFFECT OF INITIAL DENSITY ON INSTABILITY OF SAND

Fig. 4 shows a comparison of instability lines plotted on the Cambridge p' - q diagram for the two series of undrained compression and extension tests with initial relative densities of 30% and 60%. In addition, a third test series is plotted on the diagram, which is taken from Yamamuro and Lade (1996), who performed high-pressure instability tests on Cambria sand with initial relative density of 90%. As shown on Fig. 4, the slope of the instability line decreases slightly with decreasing initial relative density. This indicates for a given effective mean normal stress, loose soils may become unstable at lower deviator stress levels than dense soils. Initial relative density also affects the location of the bottom of the instability region. For a triaxial compression specimen with initial relative density of 90%, Yamamuro and Lade (1996) estimated the lower limit of the instability region to be at a deviator stress of approximately 7.5 MPa. This value decreases to approximately 3.5 MPa for a specimen with initial relative density of 60% and, as previously stated, the lower limit is further depressed for an initial relative density of 30%. Intuitively this result is expected since the tendency for compression in less dense specimens continues to dominate at lower confining pressures and thus, the lower limit of the instability region decreases with decreasing initial relative density. The bottom of the instability region in triaxial extension was not encountered for the loose and medium dense specimens, however, Yamamuro and Lade (1996) estimated the lower limit to be 6 MPa for the dense specimens.

How the initial relative density affects the slope of the instability lines is believed to be a function of the difference in the gradation of the material following isotropic compression. As shown on Fig. 5, sands with low initial relative densities undergo the most particle crushing during isotropic compression. This is evidenced by the looser specimens being more well

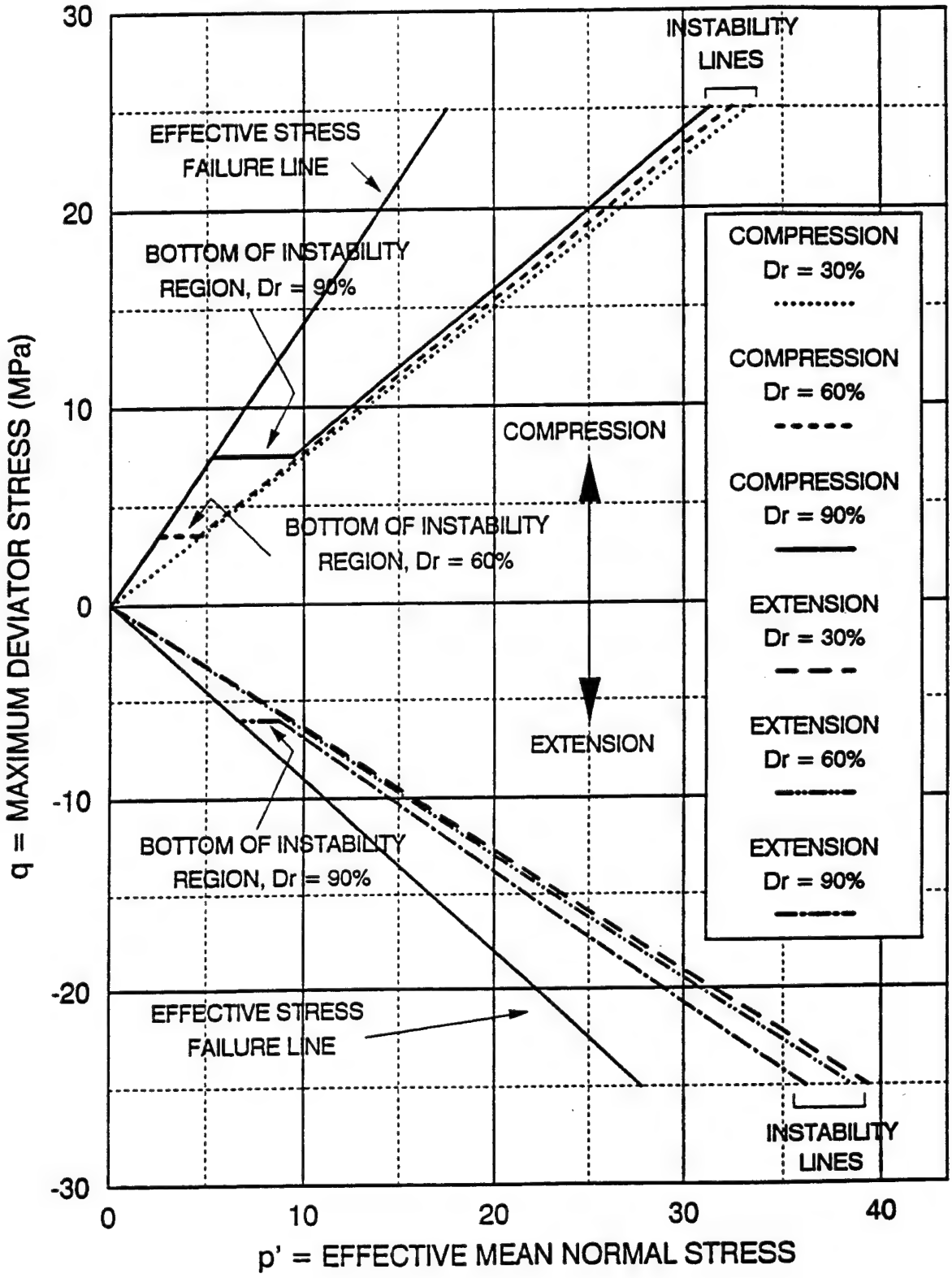

Fig. 4. Comparison of instability lines from consolidated-undrained triaxial compression and extension tests on Cambria sand with initial relative densities of 30%, 60%, and 90%.

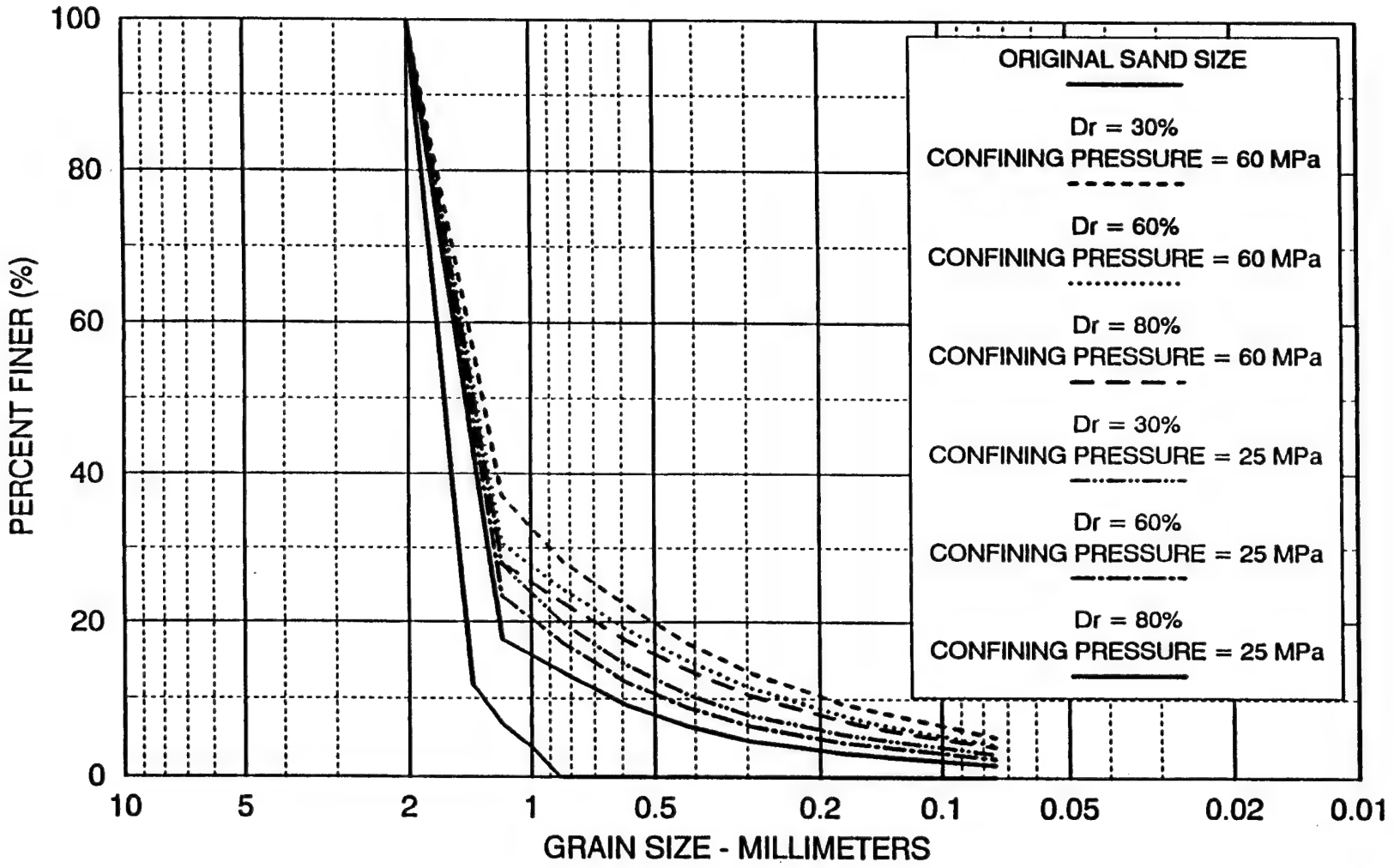

Fig. 5. Grain size distribution curves after isotropic compression tests on Cambria sand with initial relative densities of 30%, 60%, and 80%.

graded after loading up to 25 and 60 MPa. However, with increasing density a larger number of particles surround each grain. This produces a reduction in the average grain-to-grain contact stress, resulting in less breakage and ultimately a more uniform sand following isotropic compression. Since the degree of particle crushing directly affects the grain size, different density specimens consolidated to the same confining pressure will end up with different grain size distributions. In the case of undrained tests, where the maximum deviator stress is reached at very low strain values, this small variation in grain size at the beginning of shearing is believed to slightly alter the stress-strain behavior of the materials and influence the slope of the instability line.

CONDITIONS OF INSTABILITY

The region of potential instability was established for various initial relative densities of Cambria sand utilizing results from undrained triaxial compression and extension tests. Theoretically, specimens sheared to stress levels within the defined instability region should exhibit unstable behavior if undrained conditions are imposed and the load is kept constant. Such a result can be verified by performing specialized instability tests which expose specimens to states of stress both inside and outside the instability region. Special computer control programs, developed by Yamamuro (1993), were employed to perform the instability tests and determine the conditions under which a specimen exhibits unstable behavior. The control program initiated each test by first isotropically consolidating the specimen to a desired confining pressure. While holding the confining pressure constant, the specimen was sheared under strain control in a drained condition until a specific stress

ratio was attained. Depending on the nature of the test, the stress ratio related to a state of stress either inside or outside the instability region.

Upon reaching the chosen stress ratio, the specimen was turned undrained and stress control conditions initiated. Instability was indicated by the inability of the control program to hold the vertical deviator stress constant. If the behavior was stable, then the control program had little trouble maintaining the deviator stress constant.

The effective stress paths for the triaxial compression instability tests sheared to stress levels inside the instability region are shown on the Cambridge p'- q diagram on Fig. 6. These two tests were sheared to effective principal stress ratios of 2.25 and 2.75, which exposed the specimens to states of stress well within the established instability region. It was anticipated that once undrained conditions were imposed the specimens would immediately exhibit unstable behavior. As can be seen on Fig. 7(b), upon closure of the drainage valves the pore pressures rapidly built up. This caused the effective confining pressure to decline and resulted in the specimen being unable to maintain the current load, even though the computer control program attempted to maintain the deviator stress constant. As shown on Fig. 7(a), the instability is apparent nearly immediately since the deviator stress curves have relatively sharp peaks and decline rapidly after the specimen is exposed to undrained conditions. Thus, as predicted, instability does occur when undrained conditions are imposed within the established triaxial compression instability region.

Close examination of Fig. 7(b) indicates that the specimen exposed to undrained conditions at a lower stress ratio generated a larger pore pressure response. This is due to the fact that, with increased shearing to higher stress ratios, more volume change occurs during the drained shearing phase of the test and the tendency for volumetric compression (i.e. pore pressure

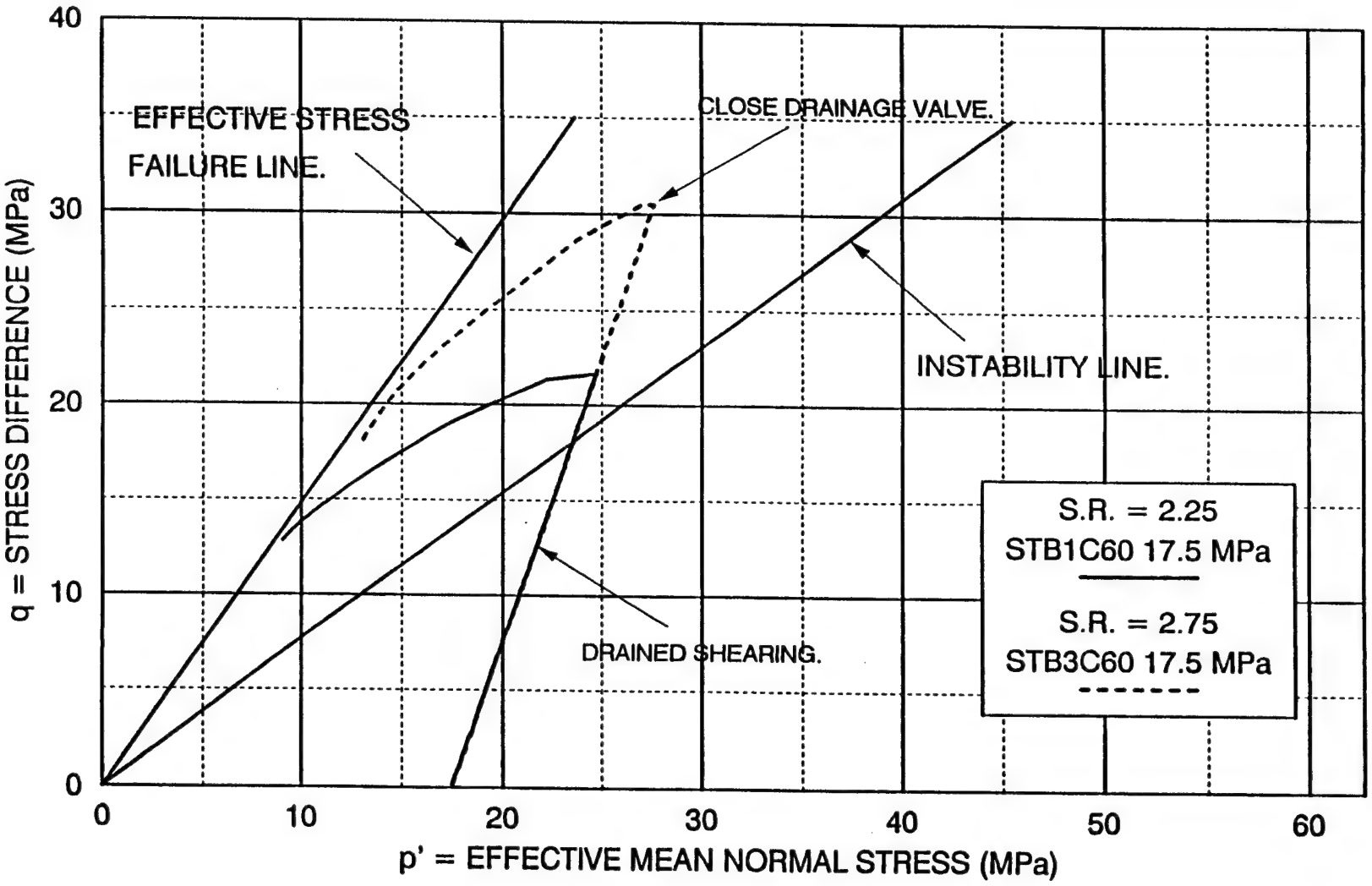

Fig. 6. Effective stress paths in p'-q diagram for two triaxial compression tests on medium dense Cambria sand (D_r = 60%) exhibing instability inside the instability region immediately when undrained conditions are imposed.

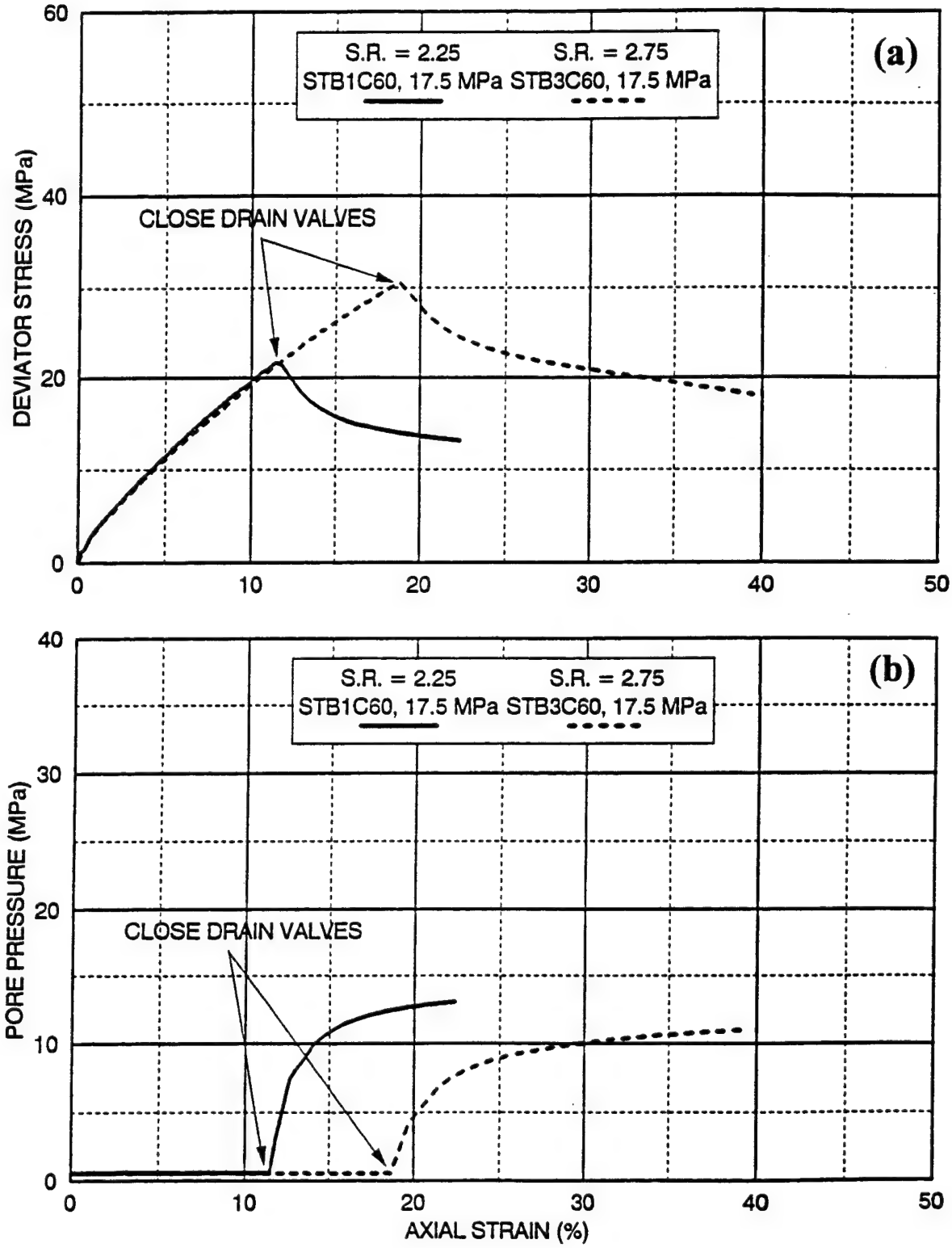

Fig. 7. (a) Deviator stress-strain and (b) pore pressure relations for two triaxial compression tests on medium dense Cambria sand (D_r = 60%) exhibing instability inside the instability region immediately when undrained conditions are imposed.

development) is reduced when undrained conditions are imposed. Also, for the lower stress ratio test, the rate of pore pressure generation is slightly greater; although both rates are seen to decrease as the effective stress path moves closer to the failure surface.

The increasing pore pressures also cause a rapid rise in the effective stress ratio curves shown on Fig. 8(a). These curves are seen to initially rise up rapidly and then increase smoothly to a maximum value at a much reduced rate coincident with the decreased rate of pore pressure development. Volumetric strains are displayed on Fig. 8(b) plotted against axial strain. The curves are seen to increase with increased shearing until the drainage valves are closed. Once undrained conditions are imposed, the curves become horizontal representing no further volume change. The initial portions of the volumetric strain curves and effective stress ratio curves overlap, which indicates good repeatability of results for tests performed at the same initial confining pressure.

The effective stress paths for instability compression tests sheared to stress levels outside the instability region are shown on the Cambridge p'- q diagram on Fig. 9. The specimens were first isotropically consolidated to confining pressures of 17.5 and 25.0 MPa and then sheared under drained conditions to effective stress ratios of 1.57 and 1.60, respectively. Once the desired stress state corresponding to a level well outside the established instability region was achieved, undrained conditions were imposed. It was anticipated that the specimens would exhibit stable behavior until the prevented volumetric creep generated sufficient pore pressure to move the effective stress path inside the established instability region. As can be seen on Fig. 10(b), once undrained conditions are imposed, pore pressures build up immediately due to the prevented volumetric creep. This causes the effective mean normal stress to decline and shift the effective stress path in a horizontal direction toward the

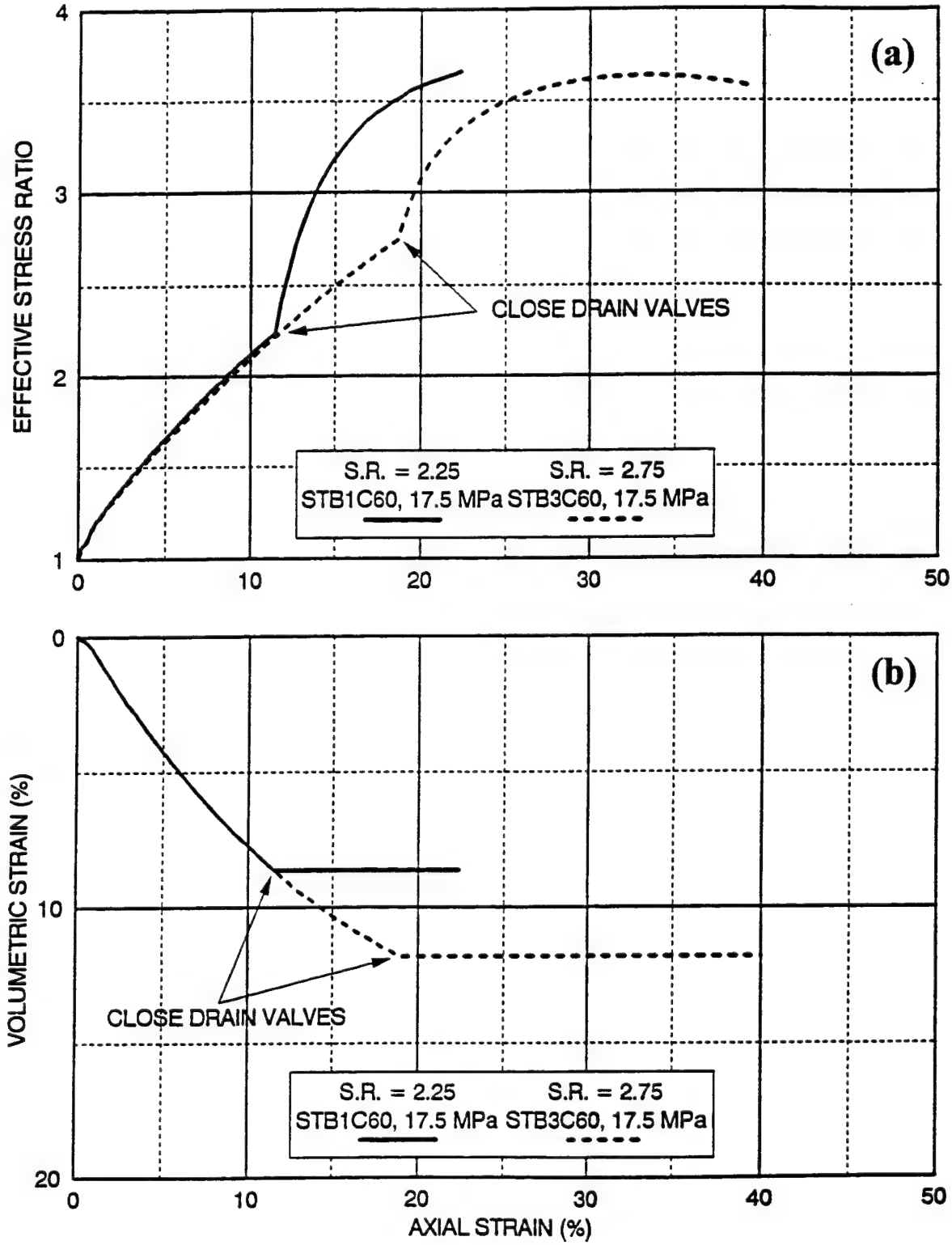

Fig. 8. (a) Effective stress ratio and (b) volumetric strain relations for two triaxial compression tests on medium dense Cambria sand (D_r = 60%) exhibing instability inside the instability region immediately when undrained conditions are imposed.

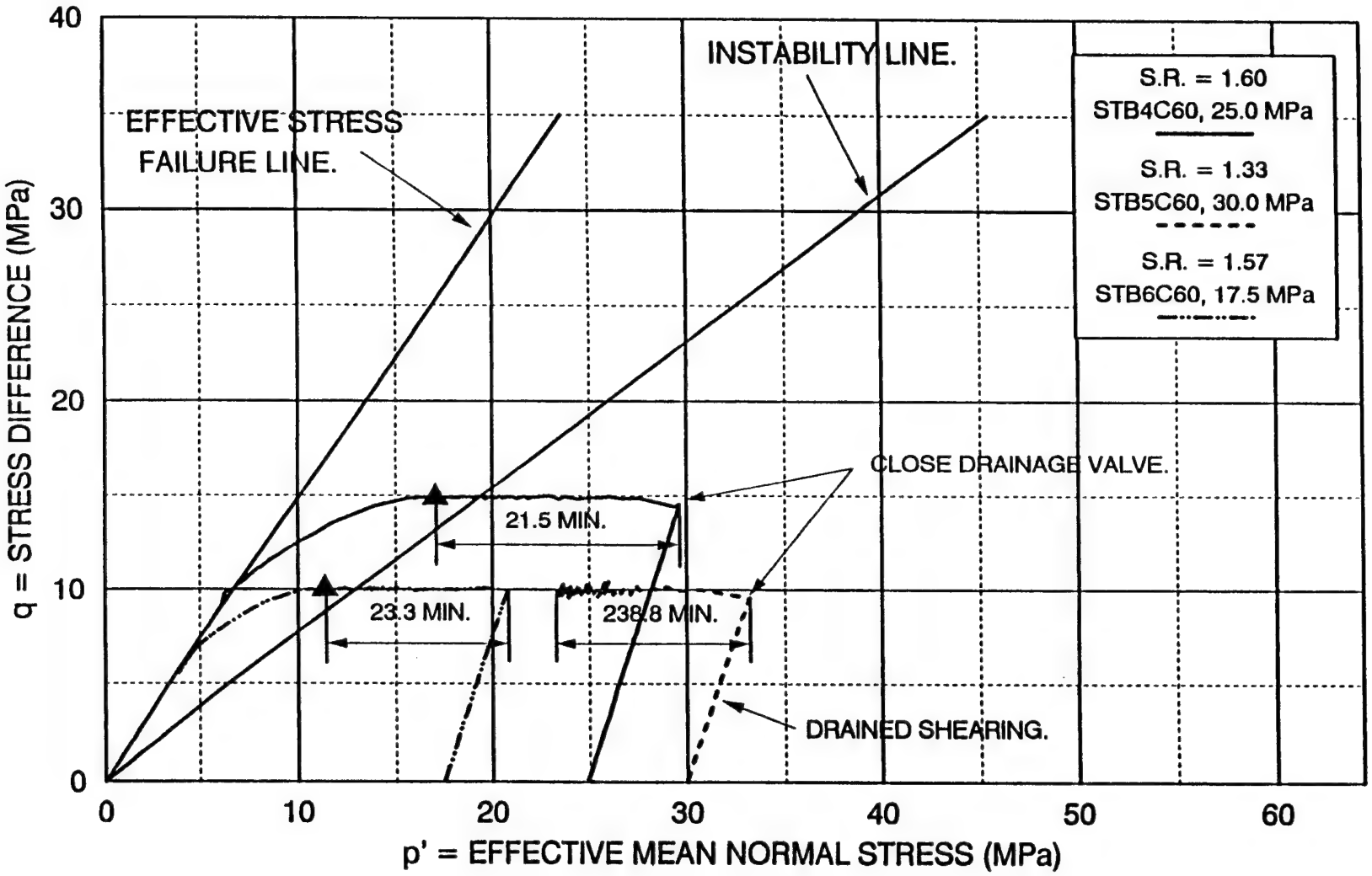

Fig. 9. Effective stress paths for three triaxial compression tests on medium dense Cambria sand (D_r = 60%) exposed to undrained creep initiated outside the instability region. Two tests eventually exhibited instability inside the instability region.

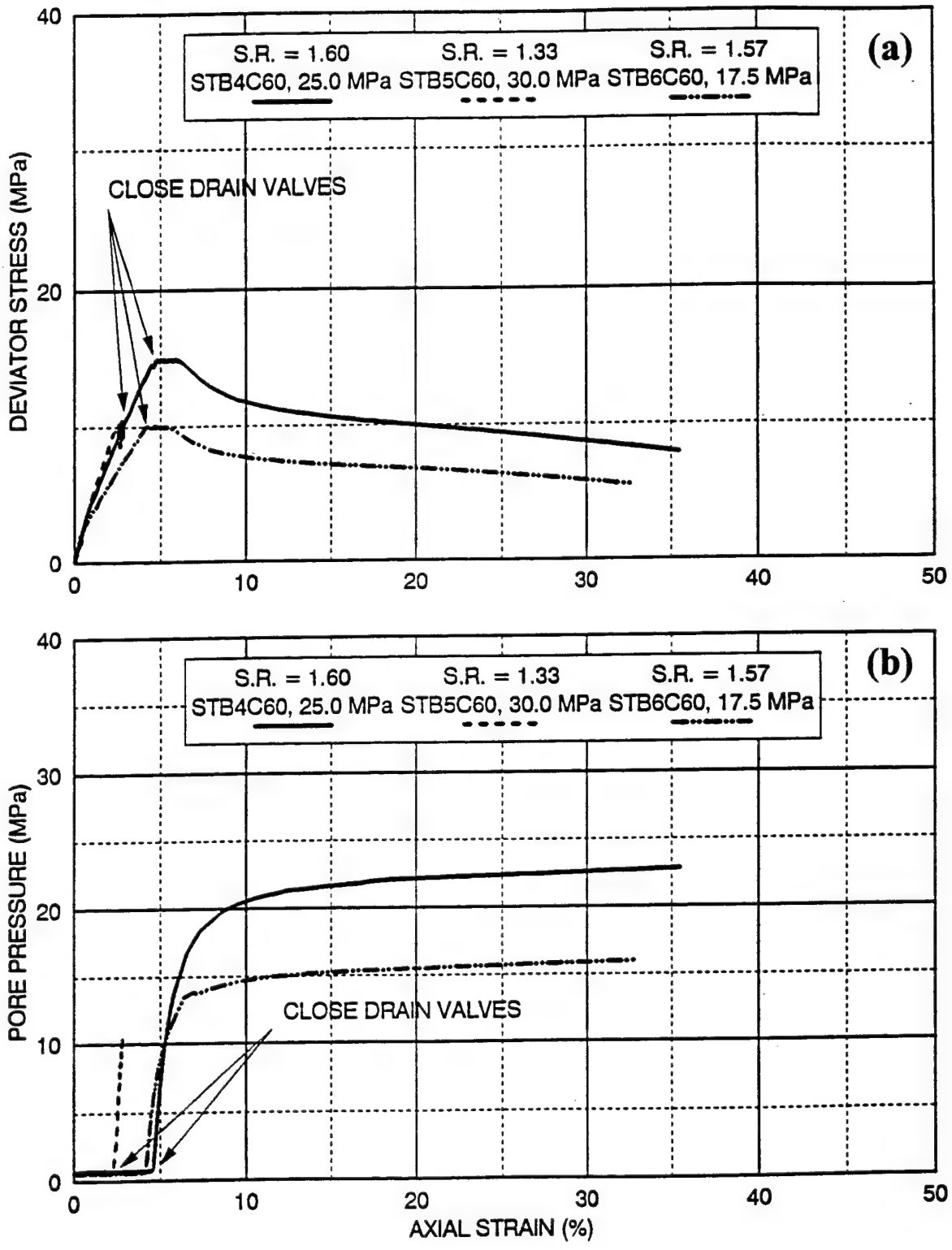

Fig.10. (a) Deviator stress-strain and (b) pore pressure relations for three triaxial compression tests on medium dense Cambria sand (D_r = 60%) exposed to undrained creep initiated outside the instability region. Two tests eventually exhibited instability inside the instability region.

instability line. Outside the instability region the deviator stress is easily maintained under stress control by the computer. This is depicted on Fig. 10(a) as the flat portion on the top of the stress-strain curves indicating a constant deviator stress. As the stress state approaches the instability line, the deviator stresses become very difficult to maintain and decline rapidly once inside the instability region, signifying unstable behavior. However, as seen in Fig. 9, instability does not occur at the instability line. Rather, it occurs when the effective stress path reaches the yield surface established when the drainage valve was closed. This is explained in further detail below.

The third test shown on Fig. 9 was performed to determine if there is a limit to pore pressure generation due to prevented volumetric creep. The specimen was consolidated to 30.0 MPa and then sheared under drained conditions to an effective stress ratio of 1.33. This stress level corresponds to a location very far outside the established instability region. As can be seen in Figs. 9 and 10(b), when undrained conditions are imposed, pore pressures increase and the stress path moves toward the instability line. However, there is a limit to the tendency toward volumetric creep, and pore pressure generation gradually reaches a maximum, and the stress state maintains a location well outside the instability line. After 238 minutes, it was obvious that pore pressure generation had essentially ceased and would not reach a level high enough to cause instability, and the test was consequently stopped.

The elapsed time from when the drainage valve was closed to the time unstable behavior initiates in the other two instability tests is also displayed on Fig. 9. The point of instability was determined by plotting the axial deformation against time on Fig. 11. The curves consist of two distinct portions: A generally flat linear section which indicates a low, consistent axial deformation rate followed by a progressively steeper section signifying an

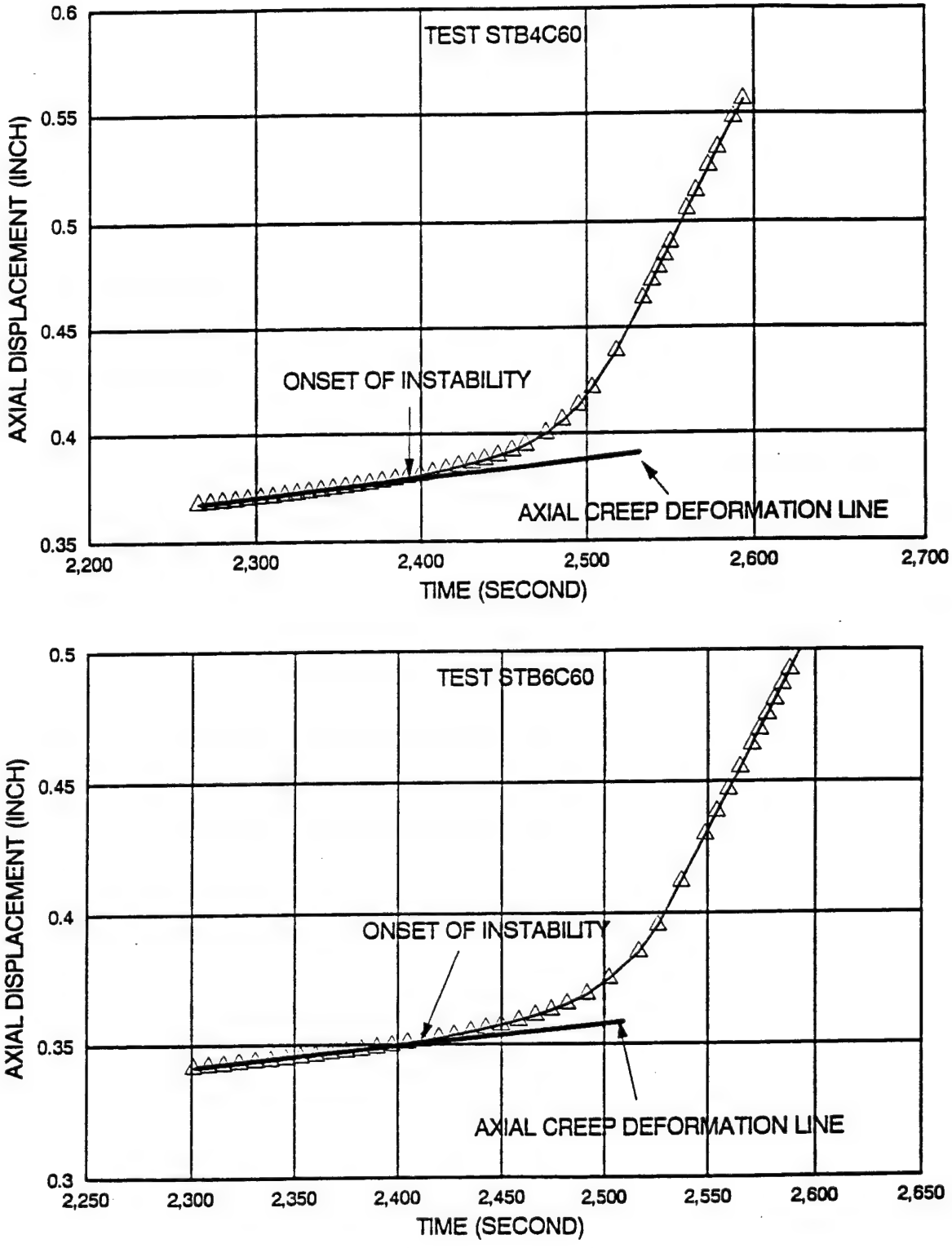

Fig.11. Determination of point of initiation of instability for two triaxial compression tests on medium dense Cambria sand (D_r = 60%) exposed to undrained creep initiated outside and creeping into the instability region.

increasing rate of deformation. The flat section occurs during undrained creep, outside the instability region, when the computer can easily maintain constant deviator stress. The curve steepens as the deformation rate is increased and the computer tries to maintain the deviator stress constant, once unstable behavior has commenced. Thus, the point at which instability initiates is located where the deformation rate curve diverges from the initially linear axial creep deformation line. This time reference is then utilized to ascertain from the test data file the effective mean normal stress at which instability begins.

The points of instability are indicated on the effective stress paths in Fig. 9 with triangular symbols. As can be seen, they fall inside the location of the instability line previously established from the undrained compression tests. This can be explained by looking at the relationship between the shape of the yield surface and the effective stress paths the instability creep tests follow. A typical yield surface for an isotropic soil is shown schematically on the Cambridge p'- q diagram of Fig. 12. Superimposed on the diagram are generalized stress paths for the instability creep tests. A specimen sheared drained to a stress state well outside the instability region will follow a stress path that goes inside the established yield surface, when undrained conditions are imposed. The sample remains stable until the stress path encounters the other side of the established yield surface, at which point the soil can deform plastically under decreasing load. As can be seen on Fig. 12, this point is well inside the instability line. On the other hand, if a specimen is sheared to a stress level in close proximity to the instability line, when undrained conditions are imposed, the soil will experience unstable behavior at or very near the instability line. As previously discussed, the instability line goes through a stress point which corresponds to $(\sigma_1 - \sigma_3)_{max}$. This point

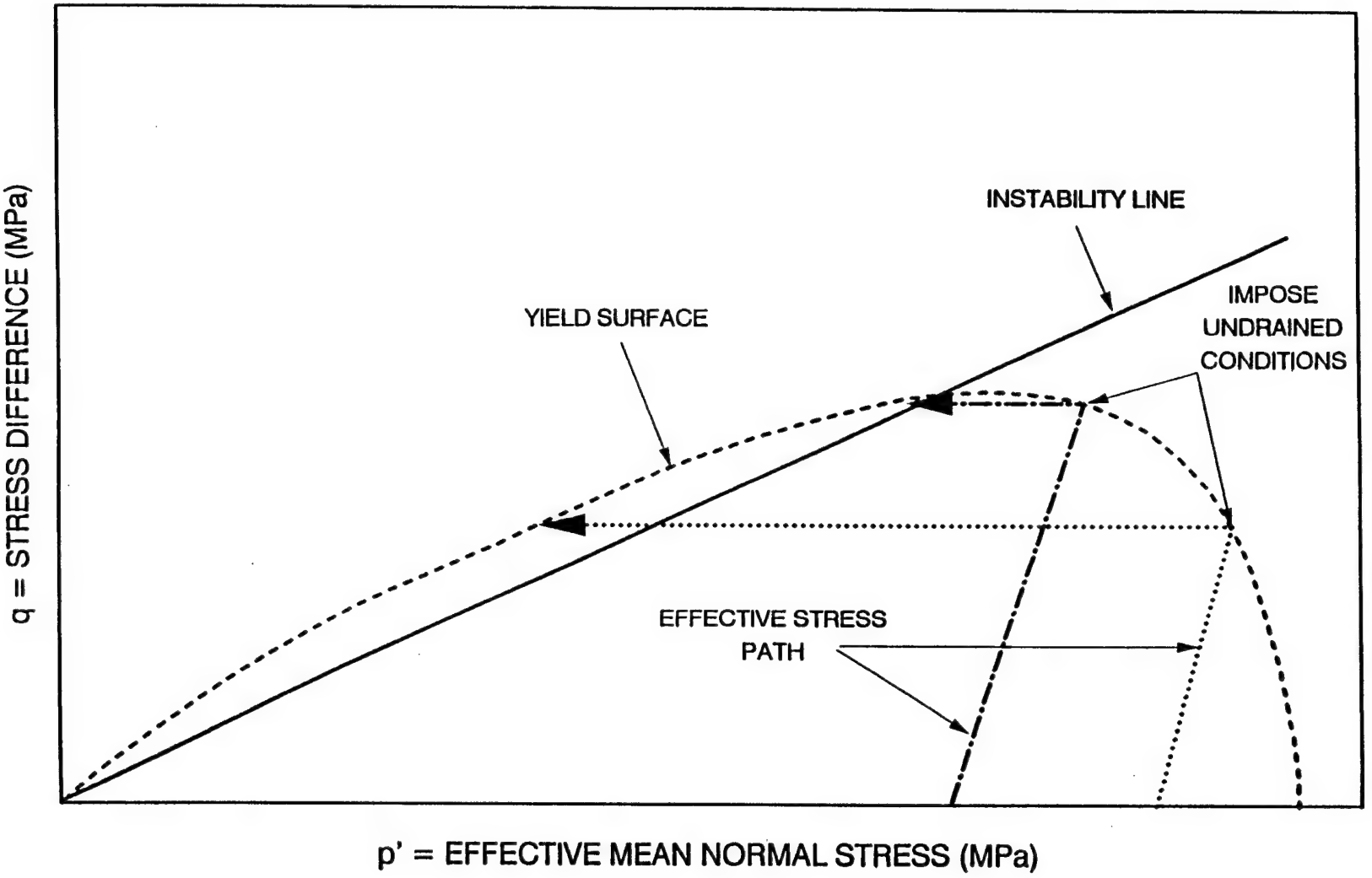

Fig.12. Relative positions of instability line, yield surface, and effective stress paths for undrained creep tests initiated outside the region of potential instability.

occurs slightly after but close to the top of the yield surface. The shape of the yield surface is nearly flat at its peak. As shown in Fig. 12, a specimen sheared to stress level in close proximity to the instability line will follow an undrained stress path nearly parallel to, but just inside the established yield surface. When the volumetric creep has generated sufficient pore pressure, the stress path encounters the instability line and yield surface nearly simultaneously and unstable behavior ensues. In this case, the point of instability will plot very close to the instability line. An example of this is shown on Fig. 13 which presents results from instability tests performed in triaxial extension.

In addition to the above instability experiments, two tests were sheared to stress ratios inside the defined instability region. The samples were held at this stress level and allowed to creep under drained conditions for either five or ten minutes before undrained conditions were imposed. Close examination of the stress paths in Fig. 14 indicates that even after undrained conditions were imposed, the deviator stress remained nearly constant for approximately 6.9 minutes following 10 minutes of drained creep, and 2.3 minutes following 5 minutes of drained creep. This is in contrast to the instability tests presented on Fig. 6 which did not undergo drained creep and immediately became unstable once undrained conditions were imposed. The effect of the drained creep was to allow stable behavior to occur inside the instability region by pushing the existing yield surface out. Once the undrained conditions were imposed, the sample did not immediately become unstable but maintained a constant deviator stress until the developing pore pressures moved the stress condition outside the newly established yield surface. Thus, the effect of the drained creep was to shift the point at which the specimen becomes unstable closer to the effective stress failure line. The points of instability for the two tests, indicated on the effective stress paths on Fig. 14 with solid triangles,

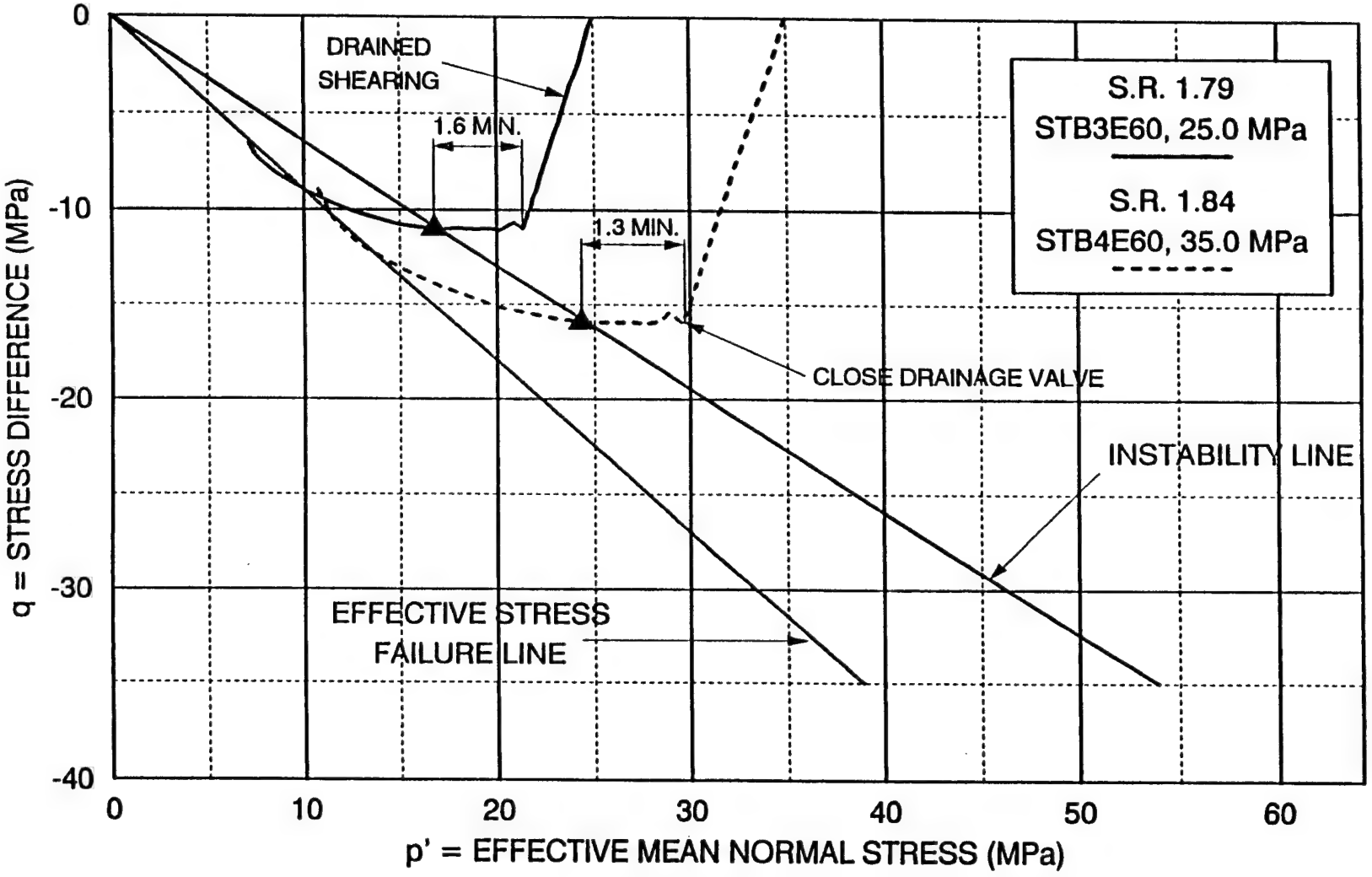

Fig.13. Effective stress paths in p'-q diagram for two triaxial extension tests on medium dense Cambria sand (D_r = 60%) exposed to undrained creep initiated outside the instability region. Both tests eventually exhibited instability inside the instability region.

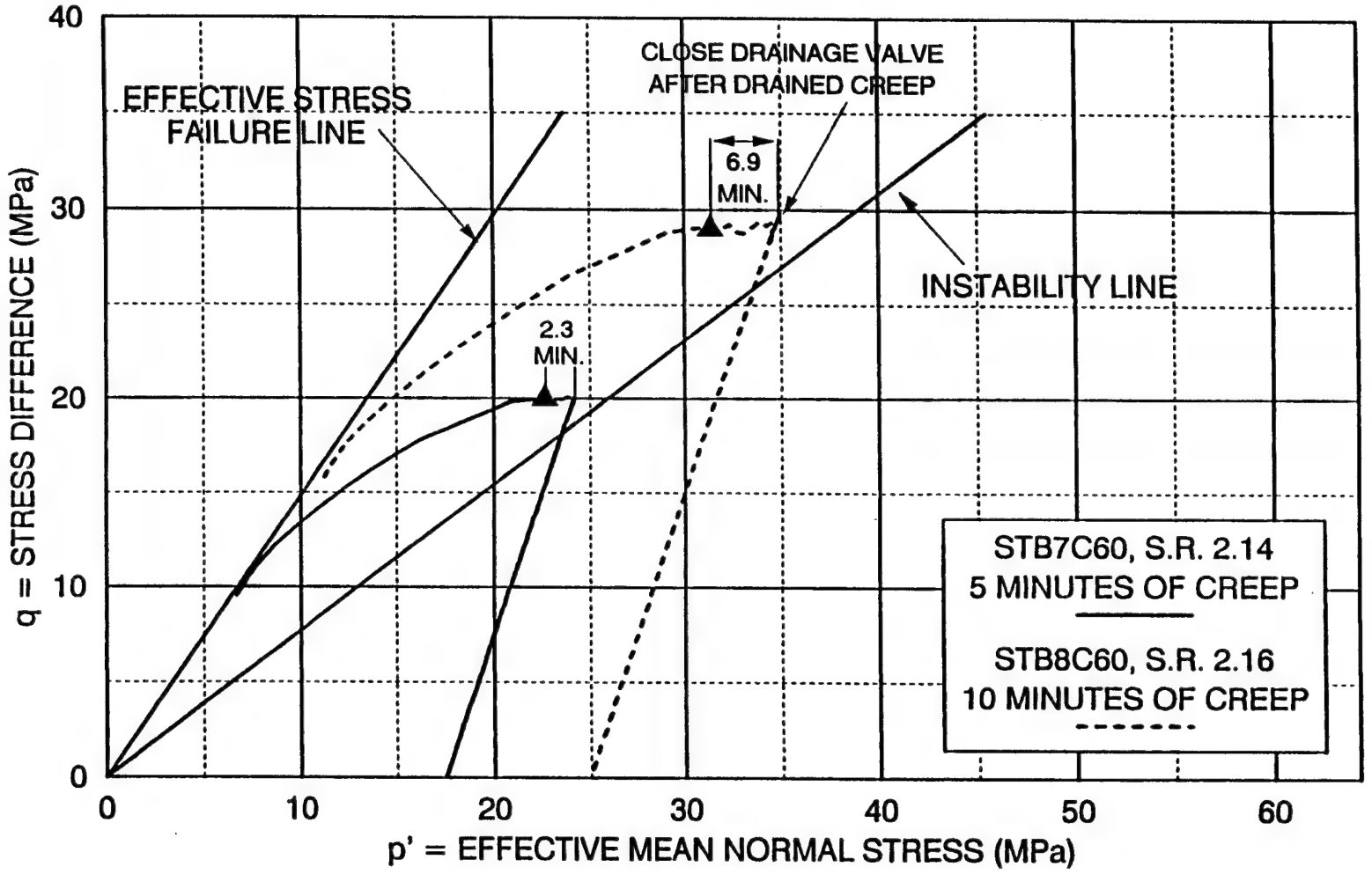

Fig.14. Effective stress paths in p'-q diagram for two triaxial compression tests on medium dense Cambria sand (D_r = 60%) initially exposed to drained creep inside the instability region before undrained creep eventually produced instability inside the instability region.

were determined as before by analyzing the axial displacement-time curves. Similar results have been presented by Lade (1994).

CONCLUSIONS

Results of undrained compression and extension tests indicate initial relative density has a small effect on the slope of the instability line. Experiments show the slope of the line decreases slightly with decreasing initial relative density. The initial relative density also affects the location of the bottom of the instability region, with the lower limit reduced with decreasing initial relative density.

The position of the instability region was experimentally confirmed by performing a series of instability tests, both inside and outside the instability region. Results of tests sheared in a drained condition to stress levels inside the established instability region show that once undrained conditions are imposed, pore pressures develop rapidly and the specimen cannot sustain the current load. Thus, unstable behavior was demonstrated and the existence of the instability region confirmed. Tests sheared in a drained condition to stress levels outside the established instability region initially exhibit stable behavior when undrained conditions are imposed. However, with continued increasing pore pressures, due to prevented volumetric creep, the stress path moves inside the instability region and the specimen becomes unstable. Again the location of the instability region was confirmed. It was found that the point of instability may plot inside the established instability line depending on the relationship between the shape of the yield surface and the effective stress path the instability test follows.

Acknowledgment

This study was supported by the Air Force Office of Scientific Research under Grant Nos. 910117 and F49620-94-1-0032. Grateful appreciation is expressed California, for this support. The experimental work presented here was performed at University of Los Angeles.

REFERENCES

Casagrande, A., 1940 (originally published in 1936), "Characteristics of Cohesionless Soils Affecting the Stability of Slopes and Earth Fills," *Contributions to Soil Mechanics*, 1925-1940, Boston Society of Civil Engineers, pp. 257-276.

Ishihara, K., Tatsuoka, F., and Yasuda, S., 1975, "Undrained Deformation and liquefaction of Sand Under Cyclic Stresses," *Soils and Foundations*, Vol. 15, No. 1, pp. 29-44.

Lade, P.V., 1992, "Static Instability and Liquefaction of Loose Fine Sandy Slopes," *Journal of Geotechnical Engineering*, ASCE, Vol. 118, No. 1, pp. 51-71.

Lade, P.V., 1993, "Initiation of Static instability in the Submarine Nerlerk Berm," *Canadian Geotechnical Journal*, Vol. 30, No. 6, pp. 885-904.

Lade, P.V., 1994, "Creep Effects on Static and Cyclic Instability of Granular Soils," *Journal of Geotechnical Engineering*, ASCE, Vol. 120, No. 2, pp. 404-419.

Lade, P.V., and Duncan, J.M., 1973, "Cubical Triaxial Tests on Cohesionless Soil," *Journal of the Soil Mechanics and Foundations Division*, ASCE, Vol. 99, No. SM10, pp. 793-812.

Lade, P.V., Nelson, R.B., and Ito, Y.M., 1987, "Nonassociated Flow and Stability of Granular Materials," *Journal of Engineering Mechanics*, ASCE, Vol. 113, No. 9, pp. 1302-1318.

Lade, P.V., Nelson, R.B., and Ito, Y.M., 1988, "Instability of Granular Materials with Nonassociated Flow," *Journal of Engineering Mechanics*, ASCE, Vol. 114, No. 12, pp. 2173-2191.

Lee, K.L., and Seed, H.B., 1967, "Drained Strength Characteristics of Sands," *Journal of the Soil Mechanics and Foundations Division*, ASCE, Vol. 93, No. SM6, pp. 117-141.

Luong, M.P., 1982, "Mechanical Aspects and Thermal Effects of Cohesionless Soils Under Cyclic and Transient Loading," *Proceedings, International Union of Theoretical and Applied Mechanics, Symposium on Deformation and Failure of Granular Materials*. Edited by P.A. Vermeer and H.J. Luger, Delft, The Netherlands, pp. 239-246,

Yamamuro, J.A., 1993, "Instability and Behavior of Granular Materials at High Pressures," Ph.D. Dissertation, University of California, Los Angeles, 738 pp.

Yamamuro, J.A., and Lade, P.V., 1997, "Instability of Granular Materials at High Pressures," *Soils and Foundations*, Vol. 37, No. 1, pp.

Experimental Study of Drained Creep Behavior of Sand

by

Poul V. Lade,[1] Member, ASCE, and Chi-Tseng Liu[2]

ABSTRACT: The experimental techniques pertaining to accurate measurement of creep in sand are explained in detail. Triaxial compression and proportional loading tests were performed in a triaxial setup for which special procedures were developed to maintain constant temperature, constant confining pressure, and constant axial load, while the axial and volumetric deformations were measured using two types of mechanical measurement systems, both free of zero drift. Special attention was paid to avoidance of air and water leakage through the membrane in the long term tests. The experiments show that the nature of creep strains is similar to that of plastic strains. They may be predicted from the framework provided by hardening plasticity theory. In particular, the potential surface determined for prediction of plastic strains may also be used for prediction of time-dependent creep strains. From the experiments it also appears that the yield surface and the plastic potential surface move out together, and the point at which to evaluate inelastic strain increment directions is at the current location of the yield surface and the accompanying plastic potential surface.

KEYWORDS: Compression, creep, drained behavior, granular material, inelastic behavior, plastic potential, sand, stress path, time effect, triaxial test

---

[1] Professor, Department of Civil Engineering, The Johns Hopkins University, Baltimore, Maryland 21218.

[2] Project Engineer, LAW/Crandall, Inc., Los Angeles, California 90040.

INTRODUCTION

Time effects such as loading rate effects, creep, and relaxation play significant roles in the behavior of soils. In geotechnical engineering projects, soil creep and relaxation are often causing long term deformation of building structures, bridge abutments, earth retaining structures, and earth slopes. Excessive deformation with time may cause structures to fail.

Inelastic work is produced during creep deformation at constant stress state. The soil seems to become harder with time while the stress state remains constant. The yield surface, defined as a contour of constant plastic work, moves in the outward direction during creep deformation. Further reloading indicates elastic behavior until the stress state reaches the current yield surface. Thus, time effects also play a role in the instability and liquefaction of granular materials. The stabilizing effect of creep on instability and liquefaction under static as well as cyclic loading can be accounted for in a rational manner (Lade 1994).

Presented here is a systematic study of creep of sand. The study includes experimentation with different strain rates, loading along different stress paths and loading with different time intervals. Tests were performed with different, but redundant measurement techniques for loads, pressures, and deformations. The study was performed (1) to investigate the nature of time effects, (2) to investigate whether the inelastic behavior in sand referred to as creep may be modeled by adding time effects within the framework provided by work-hardening plasticity theory. In particular, it is of interest to study whether the plastic potential developed for work-hardening plasticity may be employed as a potential for inelastic creep strains in sand, and (3) to provide data for development of a constitutive model for soil stress-strain-time behavior.

PREVIOUS STUDIES OF CREEP

All soils creep, but the amount of creep differs depending on the soil type. Observations indicate that creep behavior is similar in principle for all types of soil. Any increase of stresses acting on a virgin soil element produces elastic deformation (recoverable), plastic deformation (non-recoverable), and time-dependent inelastic creep deformation (non-recoverable).

Most previous studies of creep have been performed on clays, because they show considerably more pronounced time effects than most sands. This is particularly true for undrained tests, and many earlier creep experiments were performed as undrained tests. However, prevented volumetric creep in undrained tests results in further pore pressure development, which in turn causes the effective stress to change, and this results in plastic strains. Thus, undrained creep tests on clays involve both plastic and inelastic creep strains (Arulanandan et al. 1971). The externally measured, total deformations have, incorrectly, been taken to be time-dependent creep deformations. It is not possible to interpret undrained tests correctly to obtain fundamental information for development of a constitutive model for the stress-strain-time behavior of soils.

A number of studies in which drained tests have been performed on clays have resulted in great insight into time-dependent behavior of clays. Excellent reviews have been provided in the literature (see e.g. Feda 1992, Mitchell 1993, Leroueil and Marques 1996). However, clays are not very permeable, and an increase in external stress results in a pore pressure increase followed by slow dissipation with time. The effective stress, which produces time-independent plastic deformation, increases slowly corresponding to the pore pressure dissipation with time. The rate of pore pressure dissipation is a complex function of time, drainage path, and material properties. The separation of time-dependent creep deformation from time-independent plastic deformation is therefore difficult for clay. Consequently, the creep that occurs in the early stages is obscured by the uncertain separation of consolidation and creep deformations.

In comparison, sands are very permeable, and a change in external stress immediately acts as a change in effective stress in the soil skeleton. Thus, no pore pressures develop in the freely draining sand. Inelastic time-dependent creep deformations can therefore be observed immediately following stress changes and instantaneous elastic and plastic deformations. Pure creep can consequently be studied from the very beginning of its occurrence. In this respect, sands have characteristics that make experimental research on creep particularly convenient. Loose sands and sands consisting of weak particles generally exhibit more time-dependent deformation than dense sands or sands with strong particles. Creep in sands consists of slippage between grains as well as fracture of particles. Both of these effects are enhanced in loose sands with weak grains, because particle structures in loose sands are more precarious and unstable and

slippage occurs easily in such structures (Bjerrum 1973), and because more crushing occurs in loose than in dense sand (Bopp and Lade 1997).

Only few studies have been performed on time-dependent behavior of sands, and these have involved creep for relatively short periods of time (Murayama et al. 1984). A review of strain rate-dependent behavior of sands was presented by Yamamuro and Lade (1993).

EQUIPMENT AND PROCEDURES

The time-dependent behavior of sand was studied in a conventional triaxial apparatus. Modifications to this equipment were made to improve its capability to carry out long-term tests with steady stresses and accurate measurements at constant temperature. Mechanical equipment with negligible drift in applied pressures and loads and measurement systems without zero drift or devices in which the zero position could be verified during the experiments were employed for all testing.

Triaxial Equipment

The height (H) and diameter (D) of the cylindrical specimens were measured after saturation (see below), and they averaged 18.6 cm and 6.8 cm, corresponding to H/D = 2.75. Lubricated ends were employed to reduce end restraint during the long-term creep tests. By trial-and-error it was found that the system that worked best with the fine Antelope Valley sand consisted of: (1) on the cap: one thick (0.64 mm) and two thin (0.05 mm) rubber sheets with thin layers of silicone grease (Dow Corning Stopcock Grease) smeared on the end platen and between the sheets, and (2) on the base: one thick and one thin rubber sheets with silicone grease between. Cylindrical porous bronze plugs were placed in the centrally located drainage holes to prevent the specimen from sliding off the cap and base, a technique employed by Lee and Vernese (1978).

The triaxial specimen was surrounded by a 0.64 mm thick latex rubber membrane. Such a relatively thick membrane is still permeable to air and water, and to prevent air (dissolved in the

water) or water from penetrating into the specimen during the long-term creep tests, a 2-3 mm thick layer of silicone grease was smeared on the entire membrane surface in contact with the sand specimen. De-aired water was used to fill the triaxial cell, and air bubbles were removed completely through a valve in the top plate of the cell. Once practice was obtained, this technique worked well in the long-term tests (up to 3 weeks), as confirmed by comparing volume changes from two different methods of measurements.

A clear, cylindrical, triaxial cell wall made of Lucite was employed to be able to see the specimen during the test. To avoid parallax and distorted dimensions when viewing and measuring the specimen through telescopes, the cell wall was outfitted with a rectangular Lucite box attached and sealed to the outside surface of the cell wall. When the triaxial cell and the rectangular box were filled with water, the true dimensions of the specimen, free of parallax, could be viewed by eye or through telescopes.

Loading Systems

A self-compensating mercury system of the type presented by Bishop and Henkel (1962) was built to supply constant confining pressure for the present study. It consisted of three sets of mercury/water strings, each with self-compensating mercury pots, connected in series to produce a maximum pressure capacity of 1450 kPa. The first string had adjustable height capability, while the second and third strings had fixed heights. Any desired pressure could be applied to the cell through appropriate engagement and out-takes from the strings of mercury/water in the system. Back pressure was employed to help achieve and to maintain fully saturated specimens over the duration of the tests. This was supplied by regulated air pressure connected to the upper mercury pot as well as to the volume change device. Any small fluctuations of the back pressure would therefore not influence the stability of the effective confining pressure.

The vertical load was applied to the triaxial specimen either by load control for the creep tests or by deformation control for the conventional triaxial compression tests. The load control device consisted of a Bellofram (rolling diaphragm) cylinder operated by compressed air pressure. This was supplied from a compressed air bottle, which is capable of delivering stable pressure without fluctuations when controlled through two or more air pressure regulators. The

deformation rate controlled tests were performed in a 50 kN Wykeham Farrance loading machine operated by a stepper motor. This allowed determination of the full stress-strain relation including the unstable softening portion following peak failure.

Piston friction causes reduction in the accuracy of application and measurement of the vertical load as well as partial reduction in axial displacement, if not complete freeze-up of the vertical loading system. This could happen after a long period of creep where the deformation rate has reduced significantly. No correction can be applied to overcome this problem, and it is therefore important to avoid piston friction in the experimental setup. The frictionless piston seal system used for the creep tests was similar to the hydrostatic seal system designed by Chan (1975). Axial guidance for the piston was provided by two loosely fitting Teflon bushings, and the seal was provided by a balloon sealed to the piston housing with O-rings on one side and to the piston on the other side. The balloon acted as interface between the water in the triaxial cell and the air in the piston housing. Equal pressure (= cell pressure) was then applied to the inside and outside of the balloon using a piston housing seal system similar to that presented by Chan (1975).

Piston uplift was compensated in all creep tests to achieve true isotropic stress states in the isotropic creep tests as well as in the initial stages of the creep tests performed at other constant stress states. The piston uplift force (= cross-sectional area of piston times cell pressure) can be balanced by applying an equivalent downward force to the piston. This was done by attaching a cross bar to the piston and adding appropriate weights symmetrically on the two sides of the piston immediately after the cell pressure was increased.

With avoidance of piston friction and uplift force, the only correction applied to the measured load and pressure quantities was due to the force taken by the rubber membrane. This correction was calculated from the specimen strains and Hooke's law with a Young's modulus of 1400 kPa and a Poisson's ratio of 0.5.

Deformation Measurement Systems

Two systems of deformation measurements were used in this study. System no. 1 consisted of a dial gage attached to the piston for vertical deformation measurements and a

volume change device similar to that described by Chan and Duncan (1967) for measuring the amount of water expelled from or sucked into the fully saturated specimen. Strains determined from this system are compared below with those from system no. 2.

The second deformation measurement system consisted of two telescopes installed to measure the deformation between the round heads of four pins inserted through the rubber membrane at selected locations, as shown in Fig. 1. Lubricated ends were employed to ensure that the specimens deformed as right cylinders during the triaxial compression tests, as explained above. However, if end restraints were present, the barreling of the specimen may be approximated by a parabolic shape, as indicated in Fig. 1. The average lateral deformation of the parabolic shape occurs at points located 20% of the height from the ends of the specimen. Therefore, to obtain the best measurements possible, even in the presence of small amounts of friction on the end platens, the pins were placed at the points which were most likely to correspond to the average change in diameter. Nevertheless, the specimens were carefully observed throughout the tests, and they all deformed as right cylinders (within very small tolerances) up to failure. Following peak failure, some slightly irregularly shaped specimens were observed, but this was well beyond the point of interest in this study. The fact that the specimens deformed as right cylinders is also born out by the excellent comparisons between the measurements by the two systems, as presented later.

The telescope measuring device is shown in Fig. 2. It consists of two telescopes attached to positioning stages to aim at the upper and lower pins. The vertical deformation was determined by positioning each of the two stages with the help of micrometer screws that measured with a precision of 0.0013 mm. This setup was attached to a miniature linear motion ball slide to move the telescopes horizontally between two micrometer screws. These were attached to a base plate with known distance between them. To determine the lateral deformation between the upper pair of pins and between the lower pair of pins, the ball slide was moved between the two extreme positions determined by the settings of the micrometer screws. The horizontal screws each measured with a precision of 0.0025 mm. This entire setup was positioned firmly at a distance of approximately 40 cm from the specimen.

The fine cross-line reticle inside each telescope was placed by adjusting the respective micrometer screws so the lines were tangential to the round pinheads. However, the thickness of

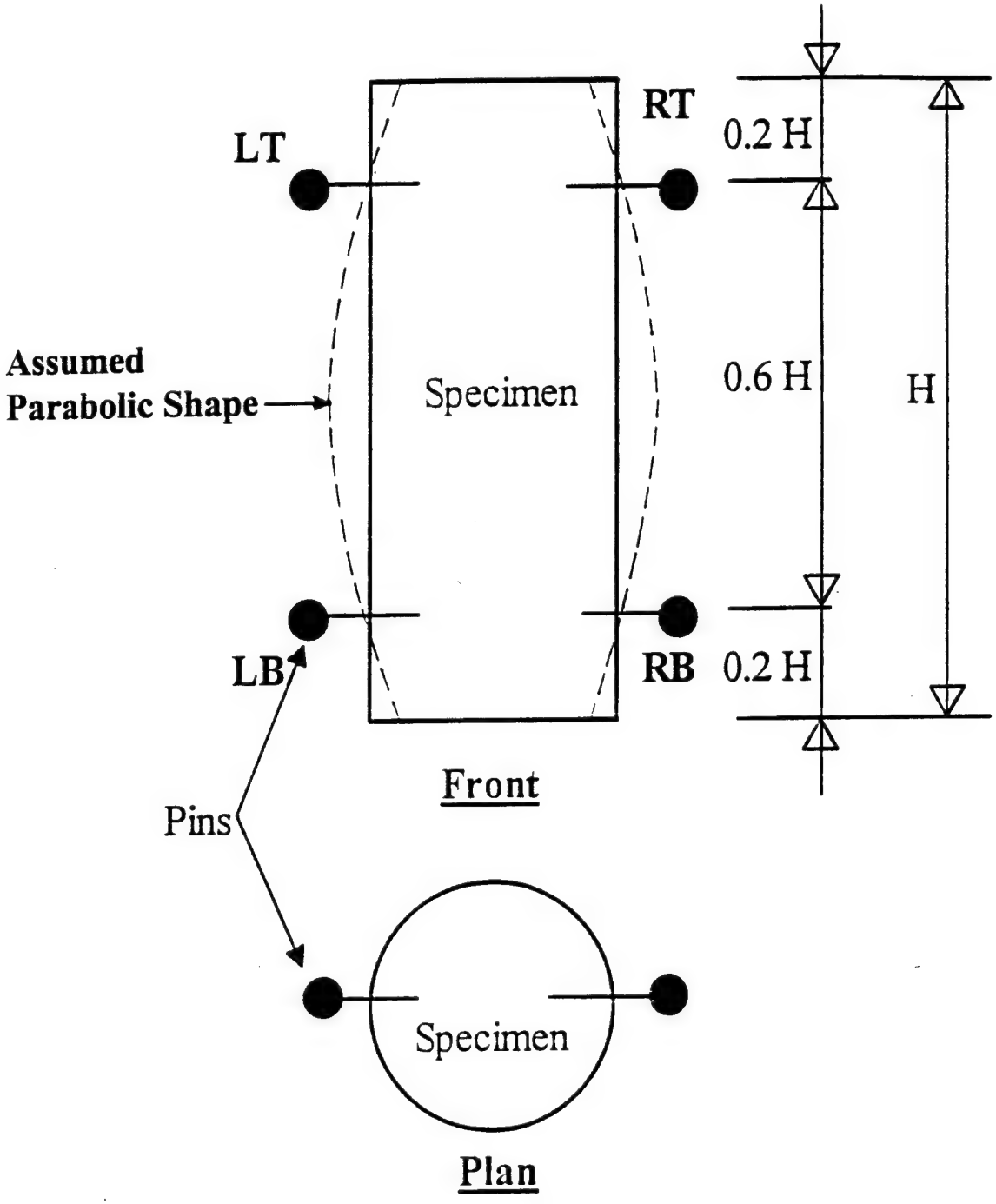

Fig. 1. Location of pins for measurement of axial and lateral deformations of cylindrical triaxial specimen.

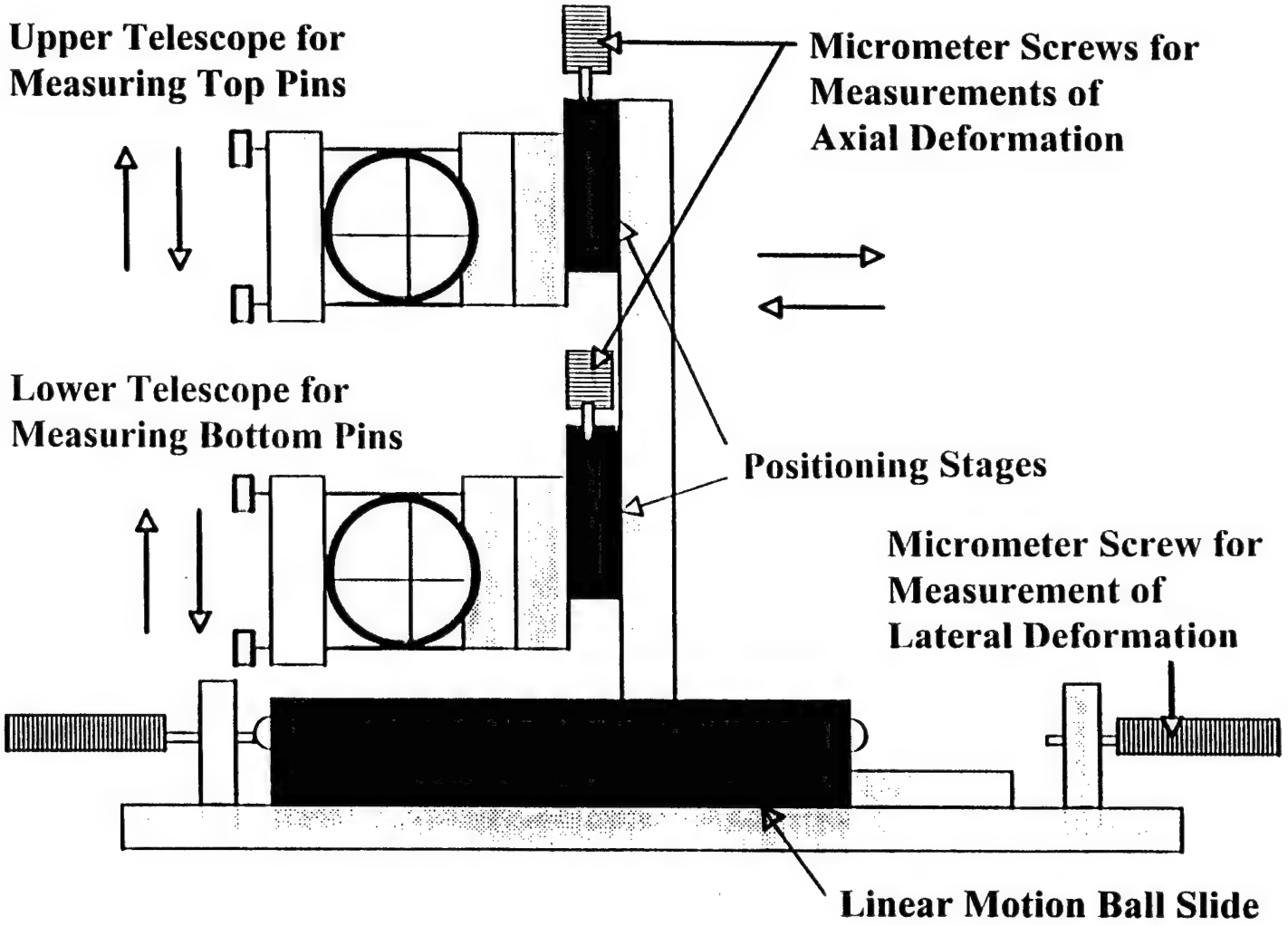

Fig. 2. Telescope device for measurement of creep deformations of triaxial specimens.

the cross-lines was larger than the precision of the micrometers, and it was difficult to adjust the micrometer screws so the lines were exactly tangential to the edge of the pinheads. Therefore, each positioning was made and recorded twice, and the average of the two readings was calculated for each pin and each direction. This was possible only after sufficient time was available at later stages in the creep experiments.

Temperature Control

Time-dependent behavior of soils has been shown to be highly dependent on temperature (see e.g. Mitchell 1993). This dependency was not investigated in this study, but it was important to maintain the temperature constant during the creep tests. In order to maintain constant temperature inside the triaxial cell, two stages of temperature control were employed. First, the temperature in the laboratory was always controlled to be below 25°C by an air conditioner operating 24 hours per day. All water used to saturate the specimen and to fill the triaxial cell was contained in a de-airing water tank in the laboratory for considerable time before it was used. Secondly, the triaxial cell and the loading machine were contained inside a Lucite chamber. A temperature control system was located inside the chamber to control the air temperature around the triaxial cell. This system included a temperature controller, a probe, and a heating device. The temperature control system was set at a temperature of 25.0°C. When the chamber temperature dropped below 24.8°C, a cartridge heater and a fan spread heated air in the closed chamber until the air had been heated to 25.2°C. Finally, a temperature recorder with a probe inside the triaxial cell measured the water temperature around the specimen. In individual creep tests the water temperature was most often observed to fluctuate by only 0.2°C, but the average temperature in each creep test varied in the range from 23.3°C to 25.7°C.

SAND DESCRIPTION AND SPECIMEN PREPARATION

Sand from the Antelope Valley north of Los Angeles, California, was used in the experimental program. The portion of sand passing U.S. sieve no. 60 (0.250 mm) and retained on

U.S. sieve no. 200 (0.075 mm) was used for the experiments. The initial grain size distribution was essentially straight between these two extreme diameters. The sand composition was determined as follows: Approximately 16% quartz, 36% feldspar, 24% biotite, 22% dense mineral (45% of the dense minerals altered to chlorite), and 2% metamorphic lithic (rock) fragments. The grain shapes were subangular. The characteristics of the sand under dry conditions are summarized as follows: Specific gravity of grains = 2.81, maximum void ratio = 1.24, and minimum void ratio = 0.98.

Specimens were prepared by dry pluviation from a height of 40 cm. This produced specimens with void ratios of approximately 1.03. The triaxial cell was then assembled around the specimen and a cell pressure of 25 kPa was applied. The specimen was then saturated using the CO_2-method. Although the specimens were apparently relatively dense, introduction of water resulted in some collapse of the soil structure, and to determine the void ratio of the specimen at this stage, the cell pressure was exchanged with an equivalent vacuum, the cell was disassembled, and the specimen dimensions were measured again. The new void ratios for the tests presented here were determined to be between 0.95 and 0.98 with an average of 0.96. Some practice was required before the specimens could be produced consistently with similar void ratios.

At this stage, the pins for deformation measurements were inserted through dabs of fluid latex rubber placed at the appropriate points on the membrane. The 2-3 mm thick layer of silicone grease was also smeared on the membrane at this time. Following this procedure, the triaxial cell was assembled again, and cell pressure and back pressure were applied to help maintain saturation of the specimens during testing. B-value tests were performed after application of back pressure, and values of 0.95 or greater were achieved to indicate satisfactory degrees of saturation of specimens for this study.

EXPERIMENTAL PROGRAM

The time-dependent behavior of Antelope Valley sand was observed for a variety of drained conditions. The testing program included studies of (1) stress-strain and strength

behavior under different, but constant confining pressures and constant strain rates, (2) effects of different strain rates on stress-strain and strength behavior, (3) creep at various stress states reached along stress paths with constant confining pressures, as shown in Fig. 3, and (4) creep at the same states of stress, but reached along stress paths with proportional loading, as also shown in Fig. 3.

Effects of confining pressure and strain rate on stress-strain and strength behavior (points 1 and 2) were similar to those observed for Cambria sand (Yamamuro and Lade 1993), and these tests will not be presented here. However, strain increment vector directions from these tests will be compared with those from the creep tests. The results and analyses of the creep tests are presented below.

EXPERIMENTAL RESULTS

Isotropic Compression

The first test to be performed in which creep was studied was an isotropic compression test. Fig. 4 shows the measured relation between the isotropic stress and the volumetric strain determined from the amount of expelled water. The specimen was prepared with an initial confining pressure of 25 kPa and compressed in increments of 49 kPa to a maximum of 785 kPa. The points (open circles) shown in Fig. 4 are those measured after 2 min of creep, at which time reasonably steady measurements could be made consistently. At the stresses where creep was studied, the initial volumetric strains measured at 0.25 min (solid circles) are shown along with the final volumetric strains (solid circles), before the stress was increased again. As creep proceeds at a given stress, the plastic yield surface moves out to higher stresses. This was realized when further loading first produces what appears to be elastic strains.

Axial and volumetric creep strains were determined from deformations measured with system no. 1 at five different isotropic stresses and shown in Figs. 5 (a) and (b), respectively. The time is doubled between measurements in order to obtain equal spacing between points on the log(time) axes in the diagrams in Fig. 5. Measurements with system no. 2 are also indicated on

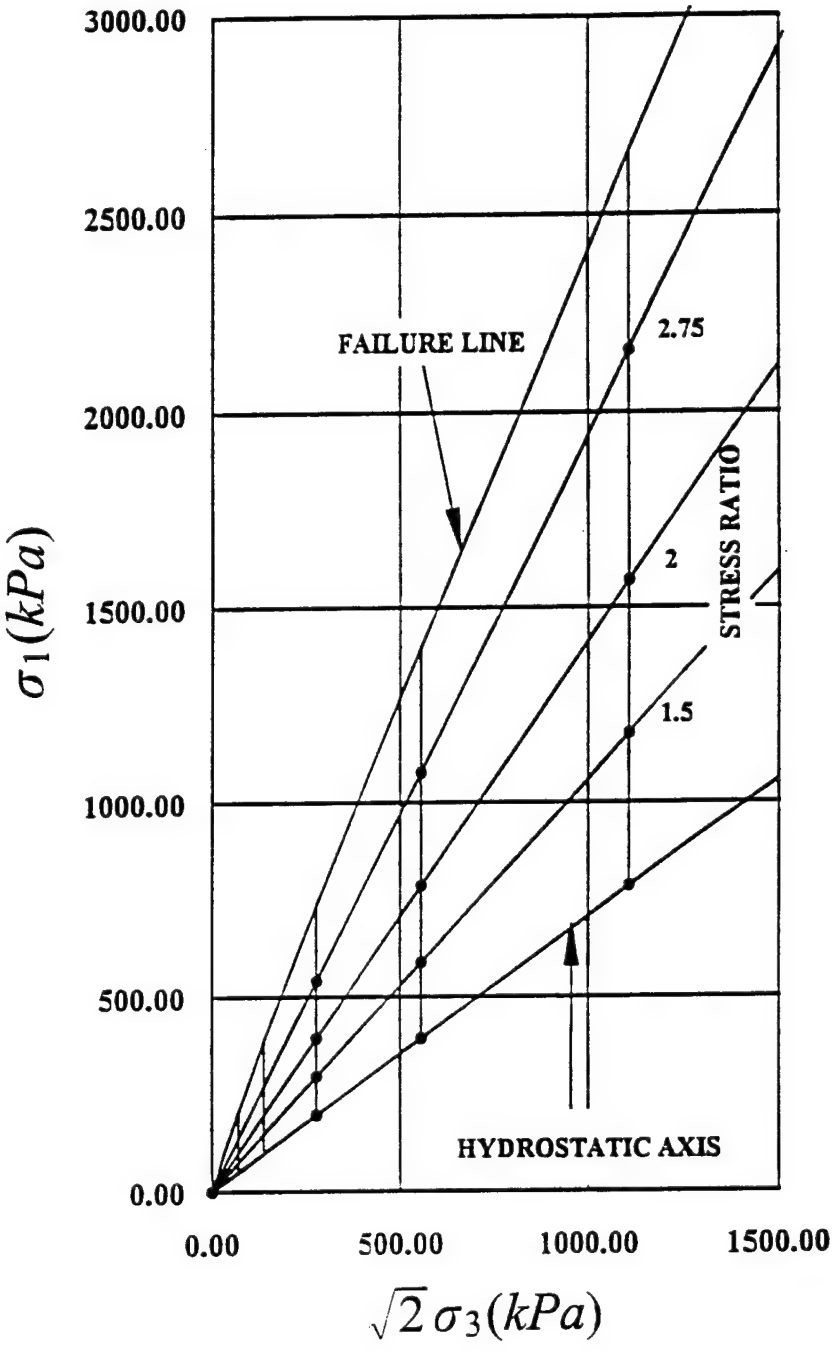

Fig. 3. Stress paths in (1) triaxial compression with constant confining pressure, and in (2) proportional loading with constant stress ratio, and stress points at which creep was measured in both types of tests on Antelope Valley sand.

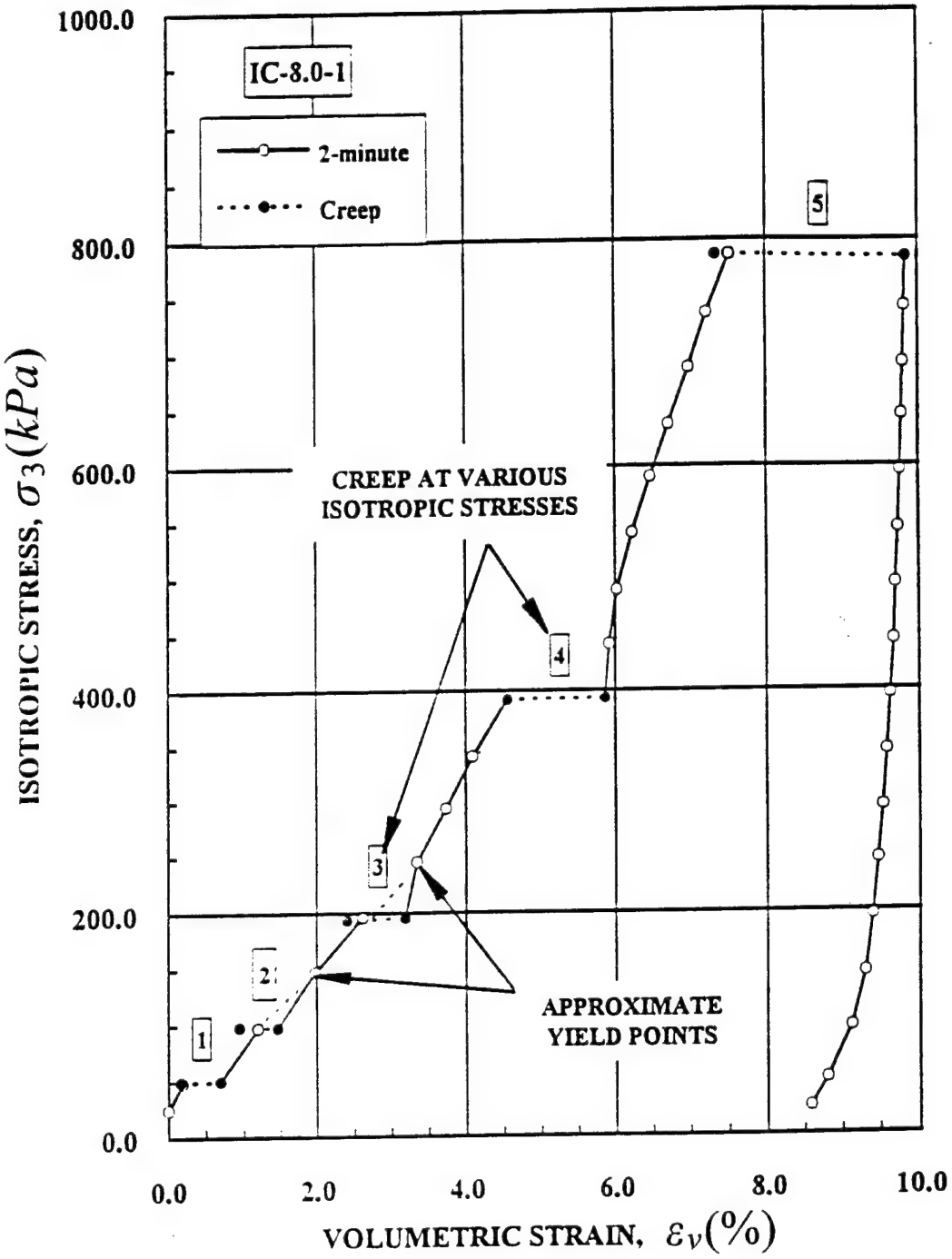

Fig. 4. Relation between isotropic stress and volumetric strain with creep at discrete stress points for Antelope Valley sand.

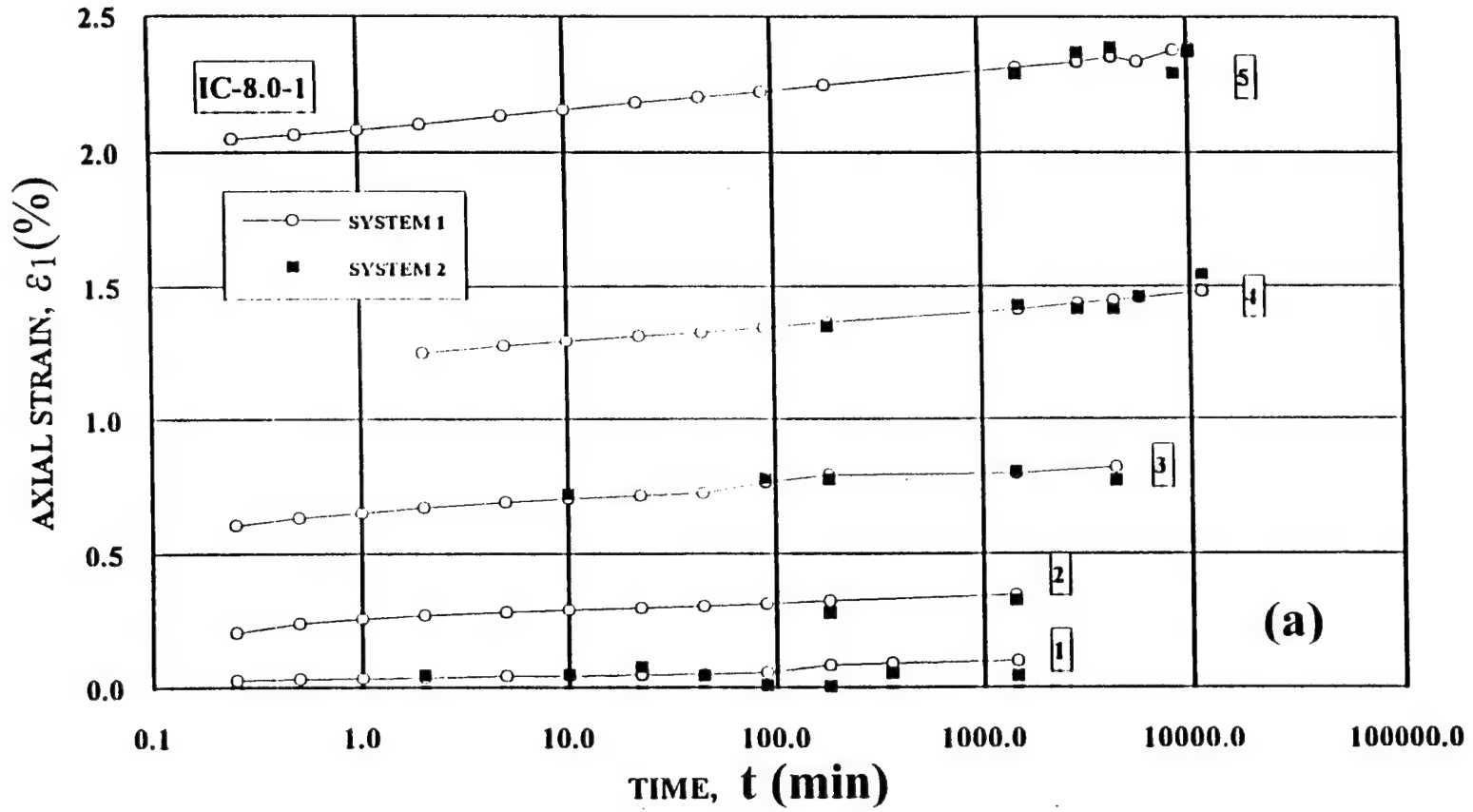

Fig. 5. Results of isotropic compression creep test showing (a) axial strain versus log(time), and (b) volumetric strain versus log(time) for Antelope Valley sand.

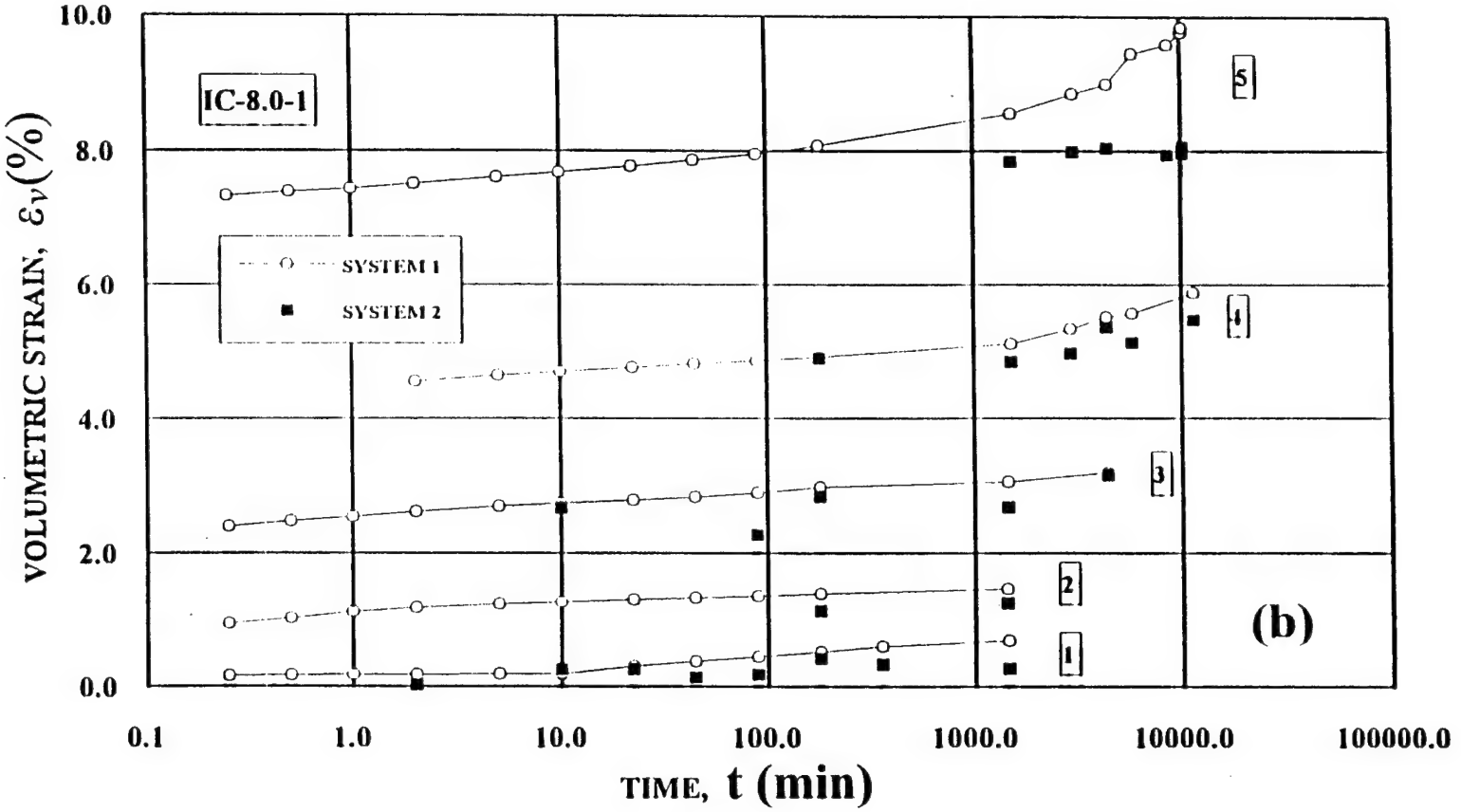

Fig. 5. Results of isotropic compression creep test showing (a) axial strain versus log(time), and (b) volumetric strain versus log(time) for Antelope Valley sand.

these diagrams at later times, when sufficient time is available for measurement with this system. Although some fluctuations occur in this first experiment, these compare very favorably with the measurements from system no. 1 during most of the test, thus confirming the quality of measurements by both systems. The data indicates an essentially linear variation of axial and volumetric strains with log(time), as has been determined before (e.g. Mitchell 1993). Thus, the rate of strain decreases with time.

However, towards the end of the 21-day long experiment, the volumetric strains determined from the expelled water at the higher pressures begin to deviate from the behavior pattern established from the earlier measurements. In comparison, the volumetric strains determined from system no. 2 still produce linear relationships. This indicates that water penetrated through the membrane and was expelled from the drained test resulting in higher volumetric strains to be determined from system no. 1, while the actual dimensions of the specimen, measured by system no. 2, would not change due to membrane leakage. Measurements by system no. 2 are therefore likely to be more correct than those measured by system no. 1 at these long testing times and high pressures. With the experience obtained from this initial experiment, improved testing procedures were established, and this produced improved quality in the remaining test series.

Comparing the axial and volumetric strains in Fig. 5 indicates that the sand behaved as an essentially isotropic material, whether due to plastic straining or due to creep. At the end of the experiment, the axial strain was 2.39% as measured by both systems, while one third of the volumetric strain was 2.69% from system no. 2. Other isotropic compression tests without creep measurements also showed that the sand behaved as an isotropic material at the given void ratio.

Triaxial Compression

Creep was studied in conventional triaxial compression tests in which the confining pressure was held constant while the stress difference was increased. The stress-strain behavior from one of these tests is shown in Fig. 6(a), and the volume change behavior is shown in Fig. 6(b). Creep observations were initiated at 5 different principal stress ratios: 1.44, 2.00, 2.77, 3.42,

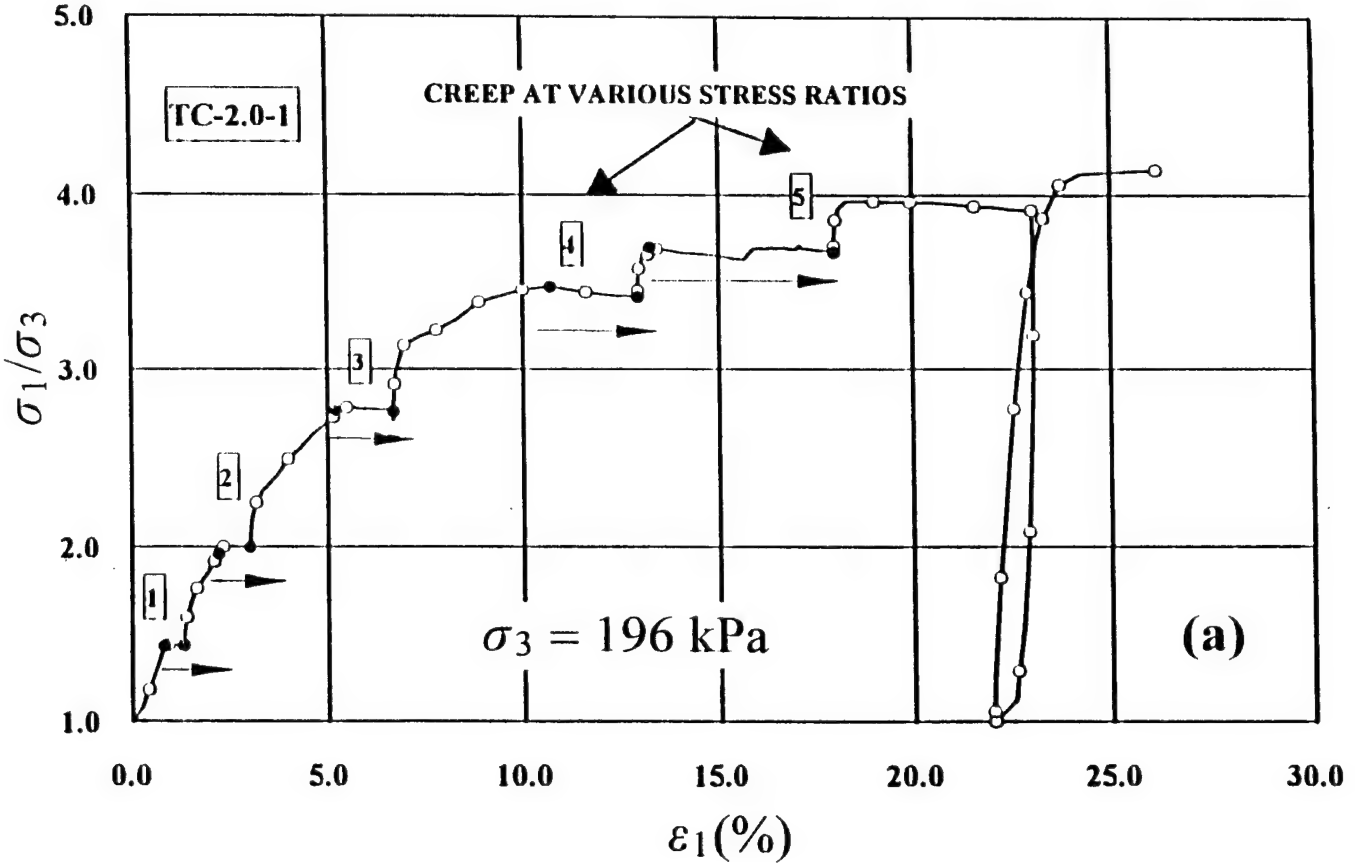

Fig. 6. Results of triaxial compression creep test showing (a) stress ratio versus axial strain, and (b) volumetric strain versus axial strain for Antelope Valley sand.

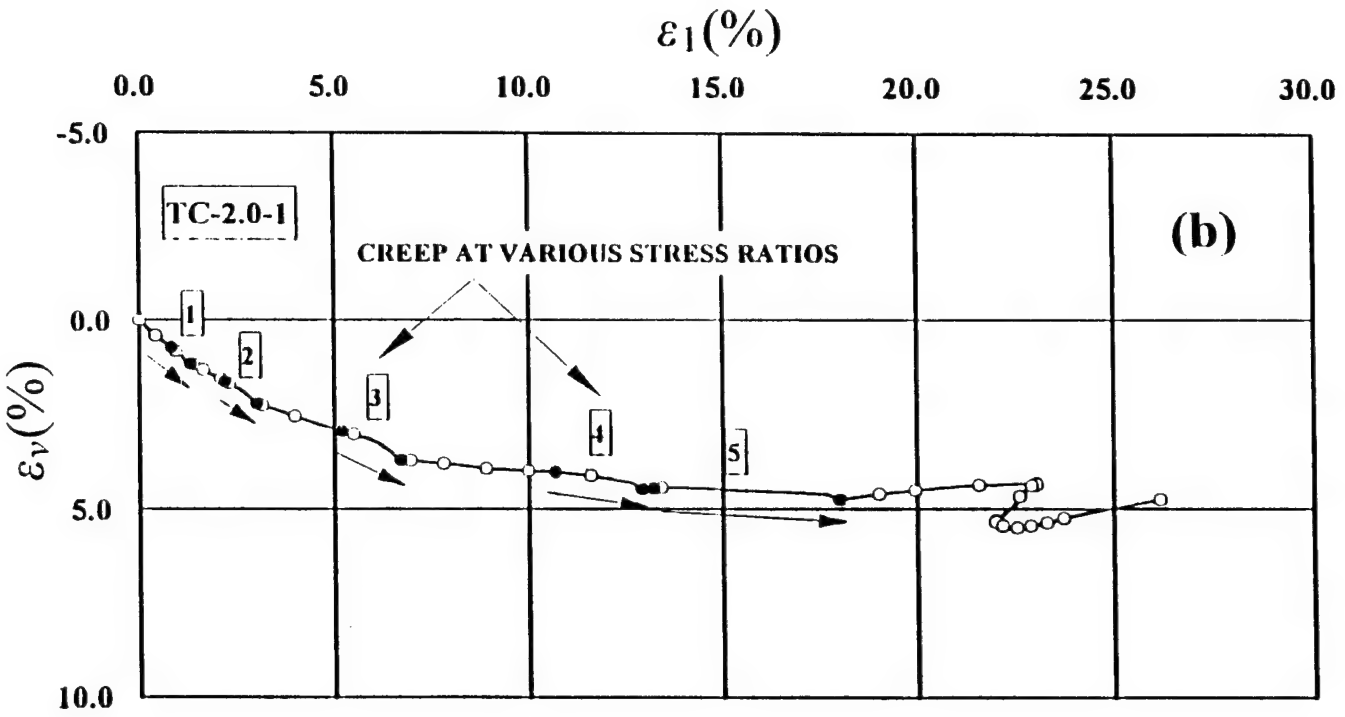

Fig. 6. Results of triaxial compression creep test showing (a) stress ratio versus axial strain, and (b) volumetric strain versus axial strain for Antelope Valley sand.

and 3.68. As in the isotropic compression test, the points (open circles) shown in Fig. 6 are those measured after 2 min of creep. At the stress ratios where creep was studied, the initial strains measured at 0.25 min are shown (solid circles) along with the final strains (solid circles), before the stress difference was increased again. Small decreases occurred in the stress difference at the higher stresses due to continued creep straining and consequent cross-sectional area increases. This is because the tests were load controlled rather than stress controlled. As creep proceeds at a given stress state, the plastic yield surface moves out to higher stresses, as observed in isotropic compression as well as in previous studies (e.g. Bjerrum 1973, Lade 1994). Fig. 6(b) show that the volumetric strain - axial strain relations during the five creep stages appear to be continuations of the volume change curve obtained during primary loading.

Figs. 7 (a) and (b) show the axial and volumetric strains plotted versus log(time) during each of the five creep stages. The strains determined from the two measuring systems are in close agreement for all stress ratios and times. Even when unusual variations occurred, as indicated by the axial strains in stage no. 5, did the two systems measure the same deformations. Thus, both deformation measurement systems worked satisfactorily. As for the isotropic conditions, linear relations are observed between the strains and log(time). Therefore, on a linear time scale the strain rates decrease with time.

Proportional Loading

Proportional loading tests were also performed in the triaxial equipment. These were carried out with constant stress ratios of 1.46, and 2.00, and with slightly varying stress ratio from 2.59 to 2.93 in the third test. The proportional loading is imposed on the specimens under load control by increasing the confining pressure and stress difference simultaneously. In each of these tests, creep was studied at the crossover points with the conventional triaxial compression tests at confining pressures of 196 kPa, 392 kPa, and 785 kPa, as indicated in Fig. 3.

Fig. 8(a) shows the stress difference versus axial strain for the test with principal stress ratio of 2.00, and Fig. 8(b) show the corresponding volumetric strain versus axial strain diagram. Following the third creep stage, the specimen was sheared to failure at constant confining pressure. As in the previous tests, the sand behaves elastically immediately during loading after

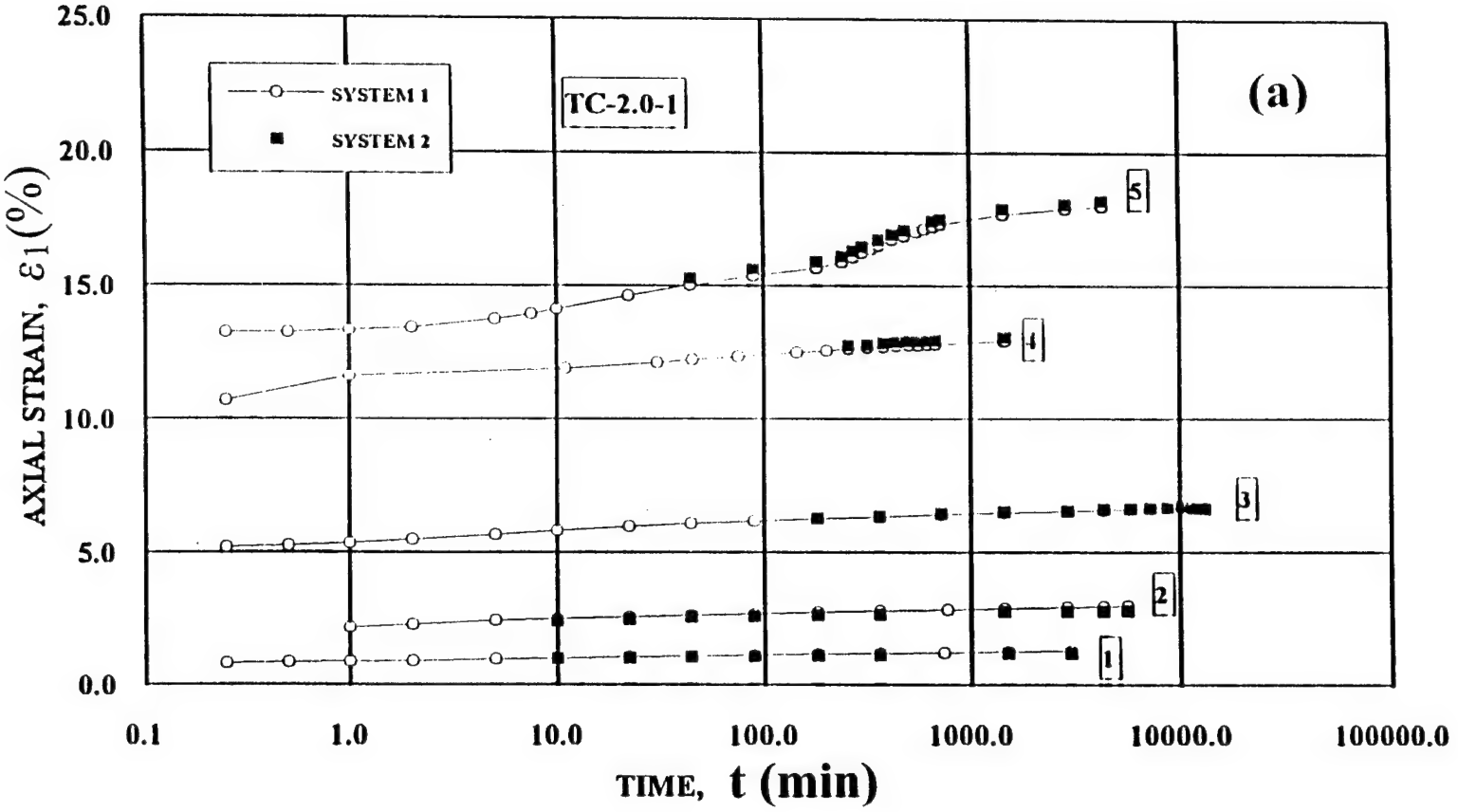

Fig. 7. Results of triaxal compression creep test showing (a) axial strain versus log(time), and (b) volumetric strain versus log(time) at five different stress levels for Antelope Valley sand.

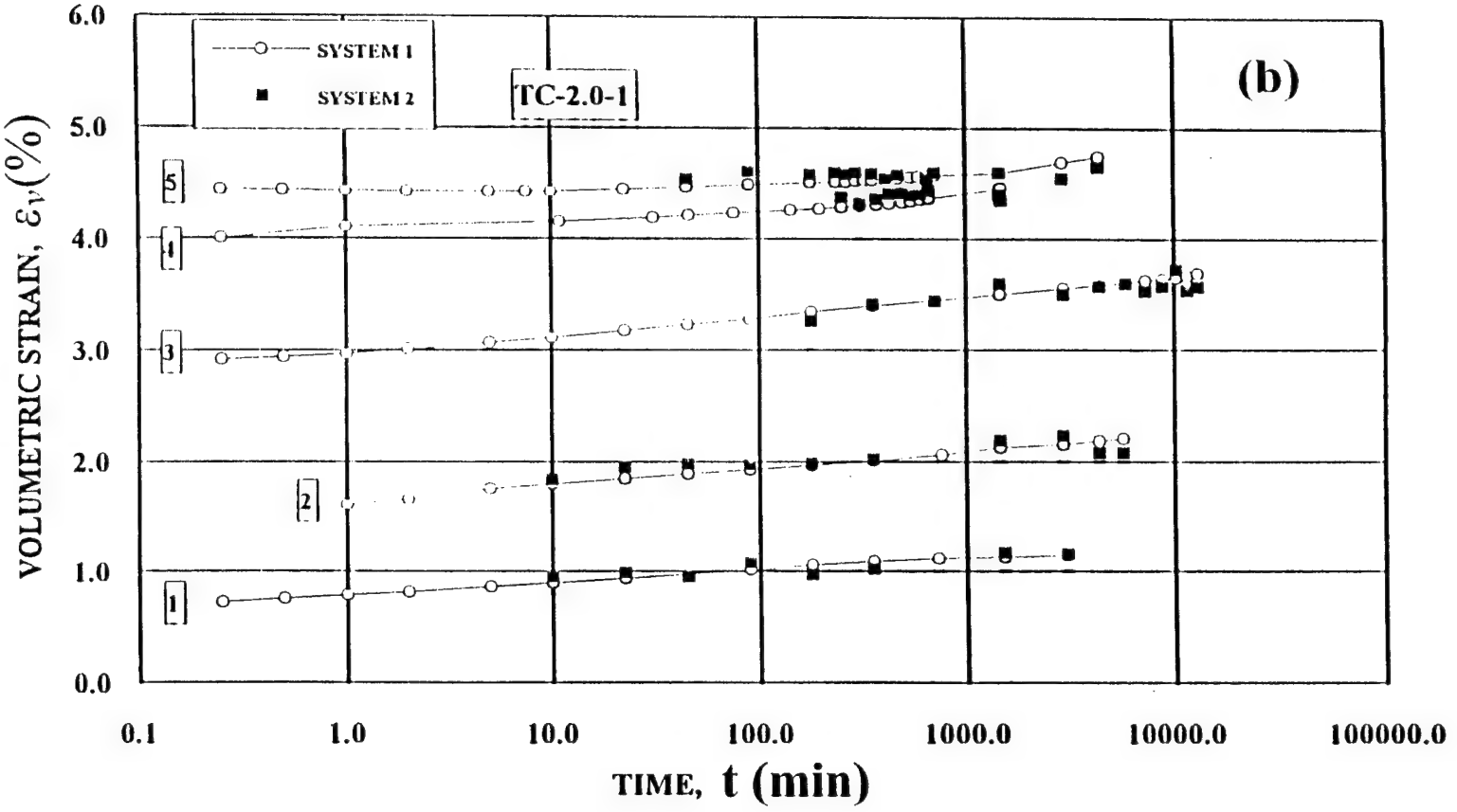

Fig. 7. Results of triaxal compression creep test showing (a) axial strain versus log(time), and (b) volumetric strain versus log(time) at five different stress levels for Antelope Valley sand.

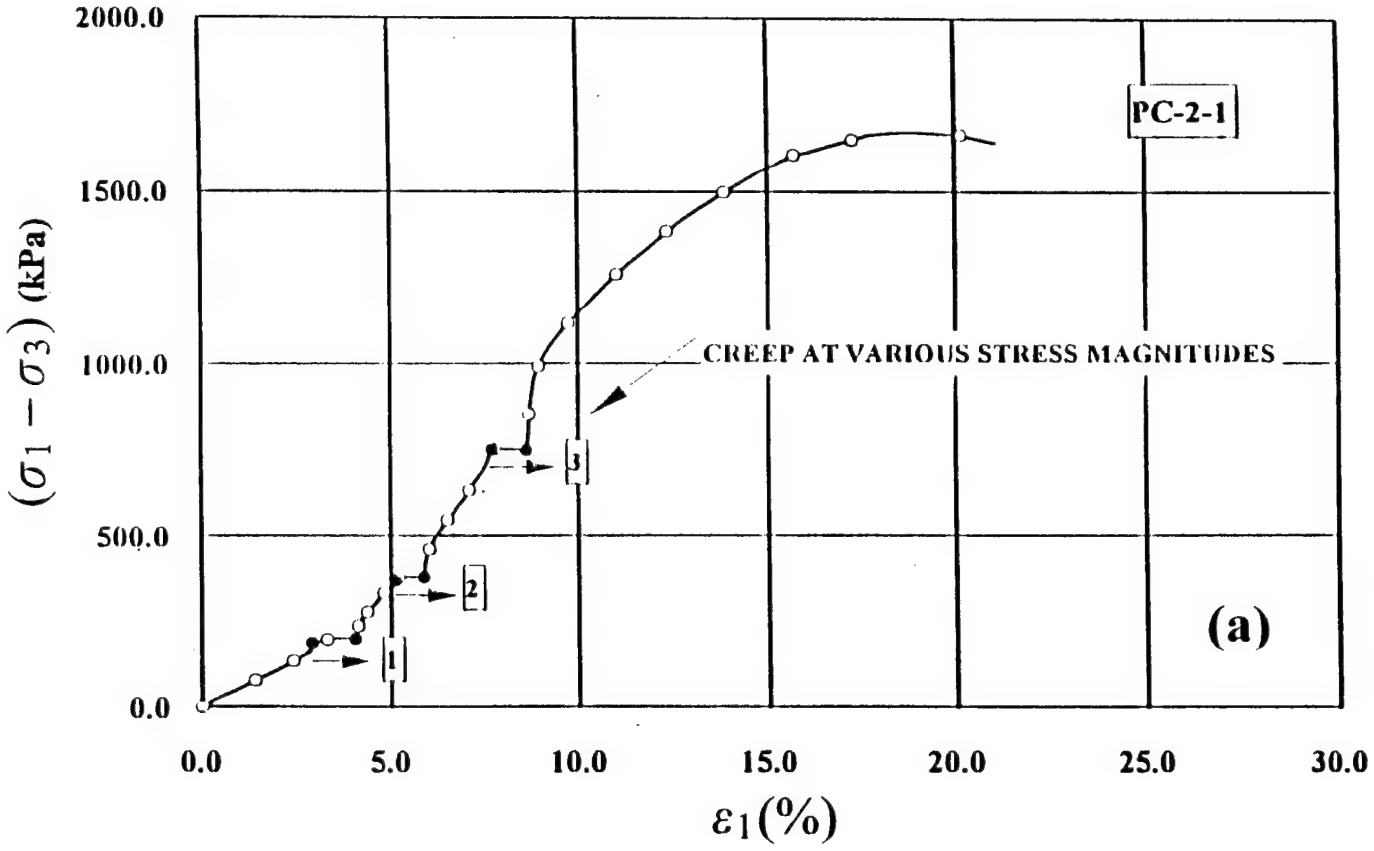

Fig. 8. Results of proportional loading creep test showing (a) stress difference versus axial strain, and (b) volumetric strain versus axial strain for Antelope Valley sand.

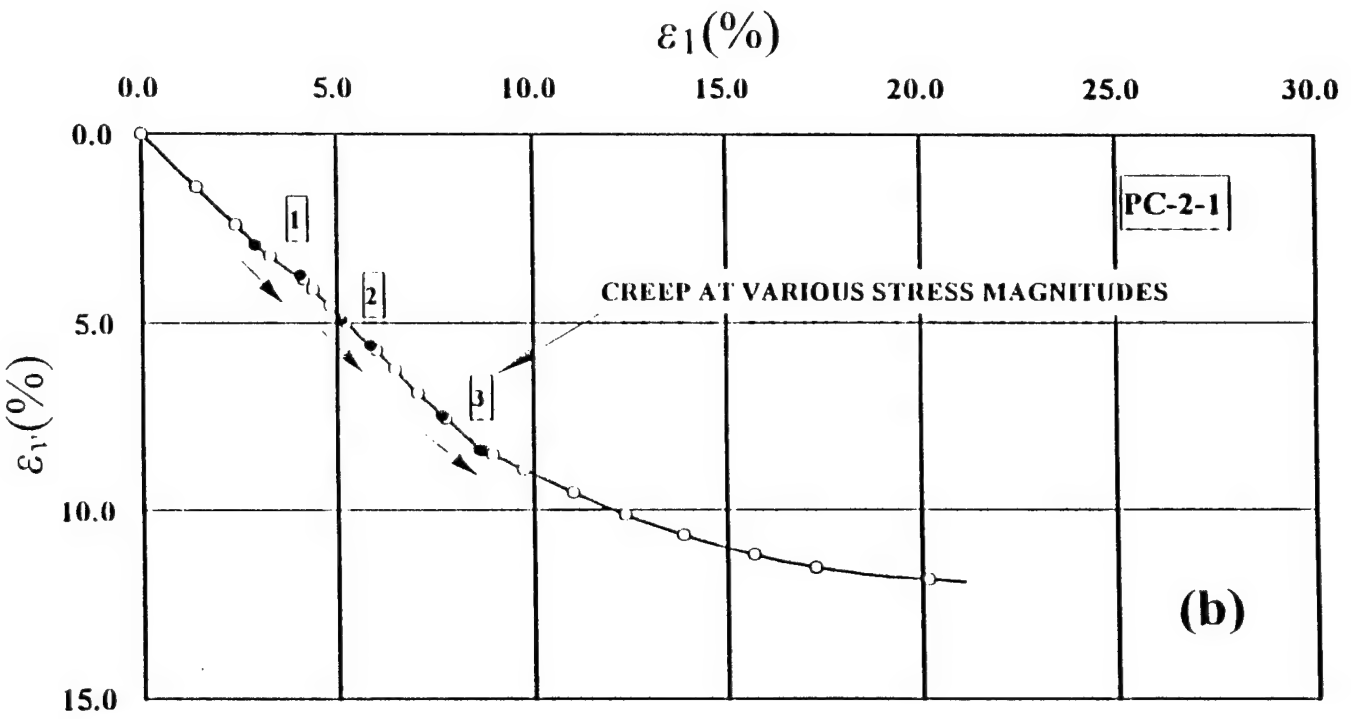

Fig. 8. Results of proportional loading creep test showing (a) stress difference versus axial strain, and (b) volumetric strain versus axial strain for Antelope Valley sand.

creep, and the volume change curve continues along the same pattern observed during primary loading. Fig. 8(b) shows that the axial and volumetric strains are very similar in magnitude, thus producing essentially zero lateral strains for a stress ratio close to 2.0. This corresponds to a value of coefficient of earth pressure at rest of $K_0 = 0.5$. This is very reasonable for this test, because the friction angel was measured to be 31.0^0 producing $K_0 = 1 - \sin\varphi = 0.485$ according to Jaky's semi-empirical formula.

Fig. 9 (a) and (b) show the axial and volumetric strains plotted against log(time) for the three creep stages in the proportional loading test. Again, the deformation measurements by the two systems are in excellent agreement throughout the entire test.

CREEP POTENTIAL

For the purpose of developing a constitutive model for stress-strain-time relations for soils, it is of interest to study whether the plastic potential employed for determination of the plastic stress-strain relationship may also be used as potential for time-dependent strains such as those observed during creep. Therefore, the strain increments obtained from the various tests in this study of Antelope Valley sand were first corrected for elastic strains as appropriate. The remaining plastic and inelastic strain increments from constant strain rate triaxial compression tests and from the creep tests reviewed above were then plotted as vector directions superimposed on the triaxial plane at the appropriate stress points.

Fig. 10 shows the plastic (time-independent) and inelastic (time-dependent) strain increments superimposed on the same triaxial plane. It may be seen that the vector directions are nearly the same at each stress point, especially at higher stress levels near failure, where the strains are largest. Vector directions are shown for two different strain rates in conventional triaxial compression tests, for triaxial compression with creep, and for proportional loading with creep. The vector directions from the conventional triaxial compression tests are most likely made up of strain increments consisting of plastic and time-dependent contributions. The vector directions measured close to the hydrostatic axis seem to be affected by the stress path direction. This may be seen by comparison of vector directions from the conventional triaxial compression

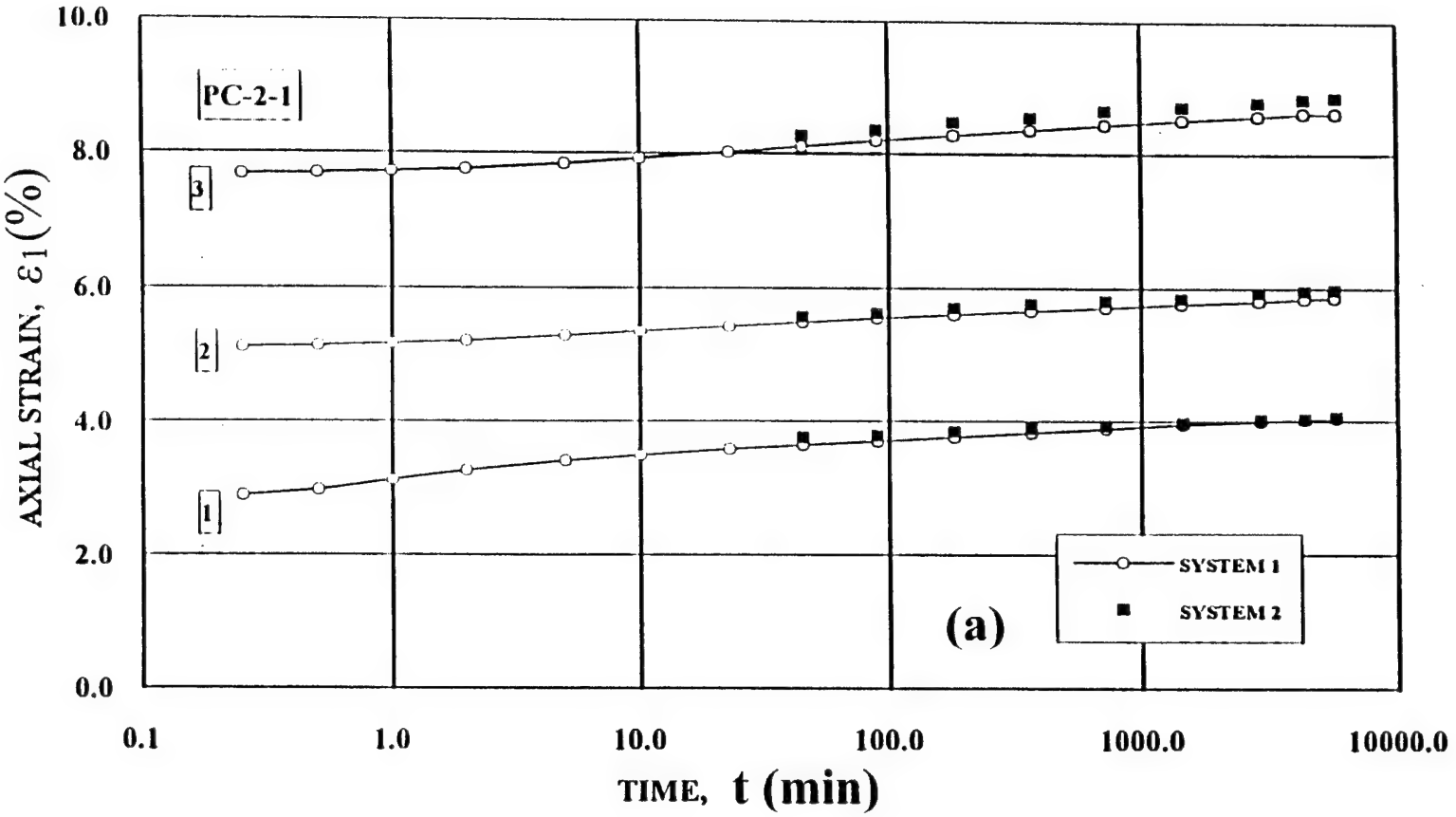

Fig. 9. Results of proportional loading creep test showing (a) axial strain versus log(time), and (b) volumetric strain versus log(time) at three different stress magnitudes for Antelope Valley sand.

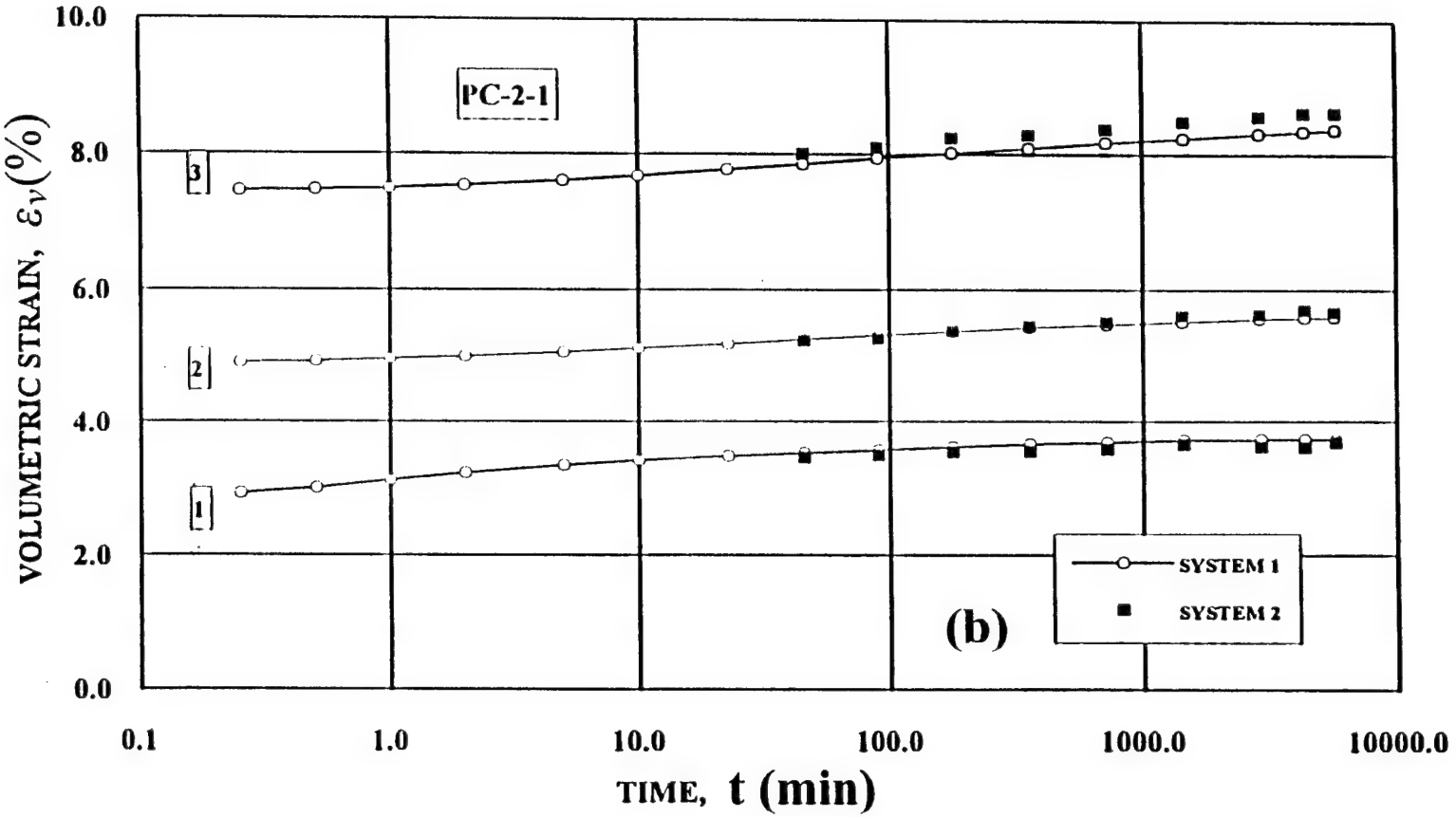

Fig. 9. Results of proportional loading creep test showing (a) axial strain versus log(time), and (b) volumetric strain versus log(time) at three different stress magnitudes for Antelope Valley sand.

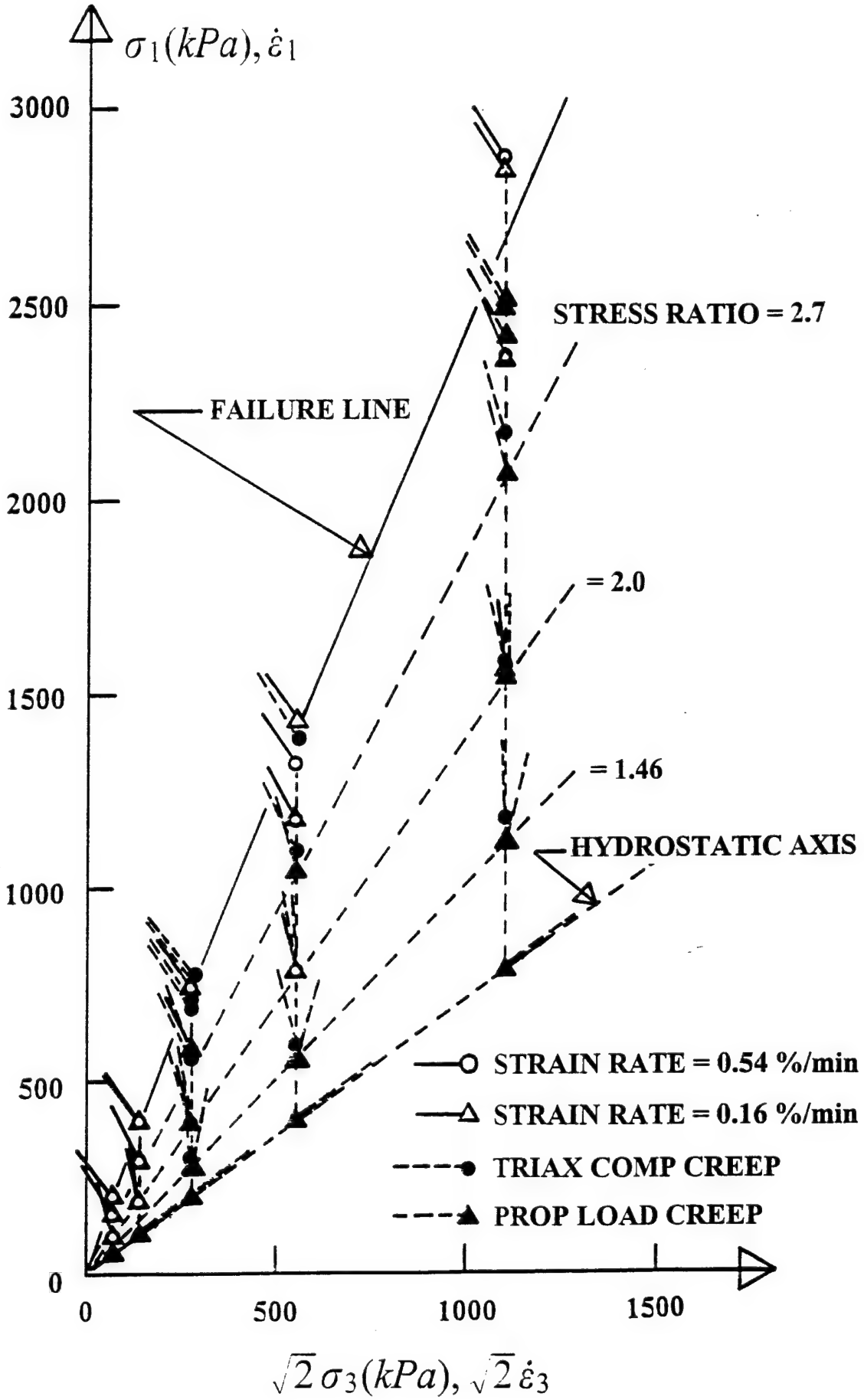

Fig. 10. Plastic and creep strain increments vectors superimposed on triaxial plane for tests in triaxial compression with different strain rates and creep at discrete points along stress paths in triaxial compression and proportional loading for Antelope Valley sand.

tests and from the proportional loading test with the lowest stress ratio (not along the hydrostatic axis). Such observations of stress path dependent behavior near the hydrostatic axis have been made before in connection with studies of directions of plastic (time-independent) strain increment directions for sand (Tatsuoka and Ishihara 1974) and their constitutive modeling (Lade and Pradel 1989). However, the strains along stress paths near the hydrostatic axis are not nearly as large as those produced closer to failure.

The observations of creep behavior in Fig. 10 indicate that the same potential surface may be employed to describe time-independent plastic strain increments and time-dependent inelastic strain increments. In order to check whether similar observations may be made for other sands, the results produced in connection with two previous studies of stability and instability of granular materials (Lade et al. 1987, 1988) were analyzed. In one study, creep was observed for up to 60 min at various stress states imposed to study stability of a dense, fine silica sand. Fig. 11 show plastic and inelastic creep strain increments for the dense sand superimposed on the triaxial plane. The dense sand dilated during shearing as indicated by the vector directions pointing towards the stress origin. The diagram shows that the creep strain increment vector directions, within the scatter of the data, are parallel with the plastic strain increment vector directions along the entire stress path. Both directions can therefore be derived from the same potential function, namely that already determined for the plastic strain increments.

Similar data were obtained in another study, and Fig. 12 shows comparison of the inelastic creep and plastic behavior in a triaxial compression test on loose Sacramento River sand. These results, which indicate sand contraction during shear corresponding to vector directions pointing away from the stress origin, also confirm that the same potential function can be used for derivation of both inelastic creep and plastic strain increment vector directions.

Figs. 13 (a) and (b) present the directions of inelastic strain increment vectors with time for Antelope Valley sand in terms of the variation of the angle β, defined on the insert in the diagrams. The angle β is measured in the clockwise direction from the abscissa in the triaxial plane to the positive direction of the strain increment vector. The vector directions shown for Antelope Valley sand in Fig. 10 are those corresponding to 2 min of creep. The results shown in Figs. 13 (a) and (b) are typical of those measured in the experiments. After the stress increase and the initial vector direction is established, the angle tends to increase slightly, indicating a

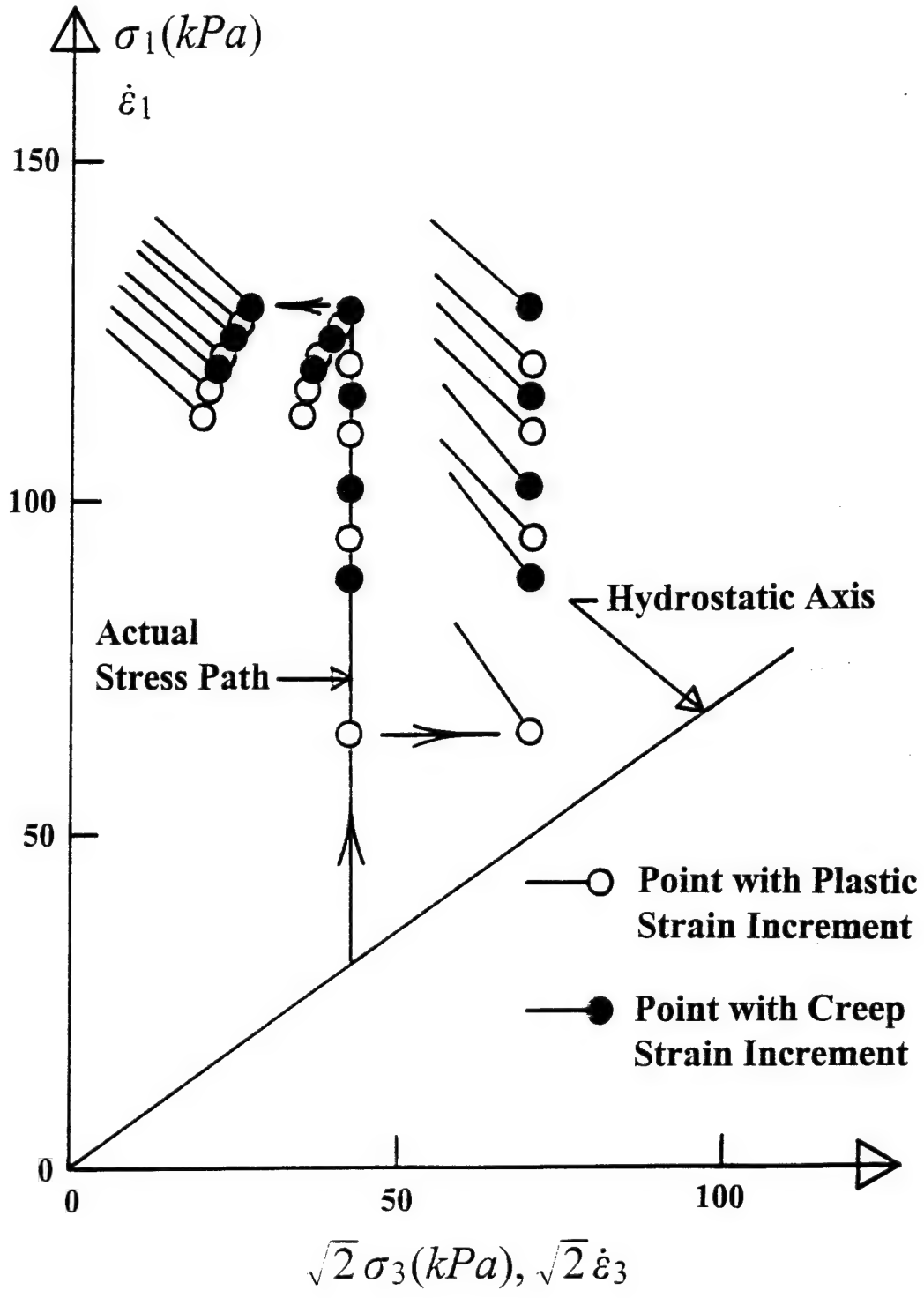

Fig. 11. Plastic and creep strain increment vectors superimposed on triaxial plane for triaxial tests performed to study stability of dense, fine silica sand.

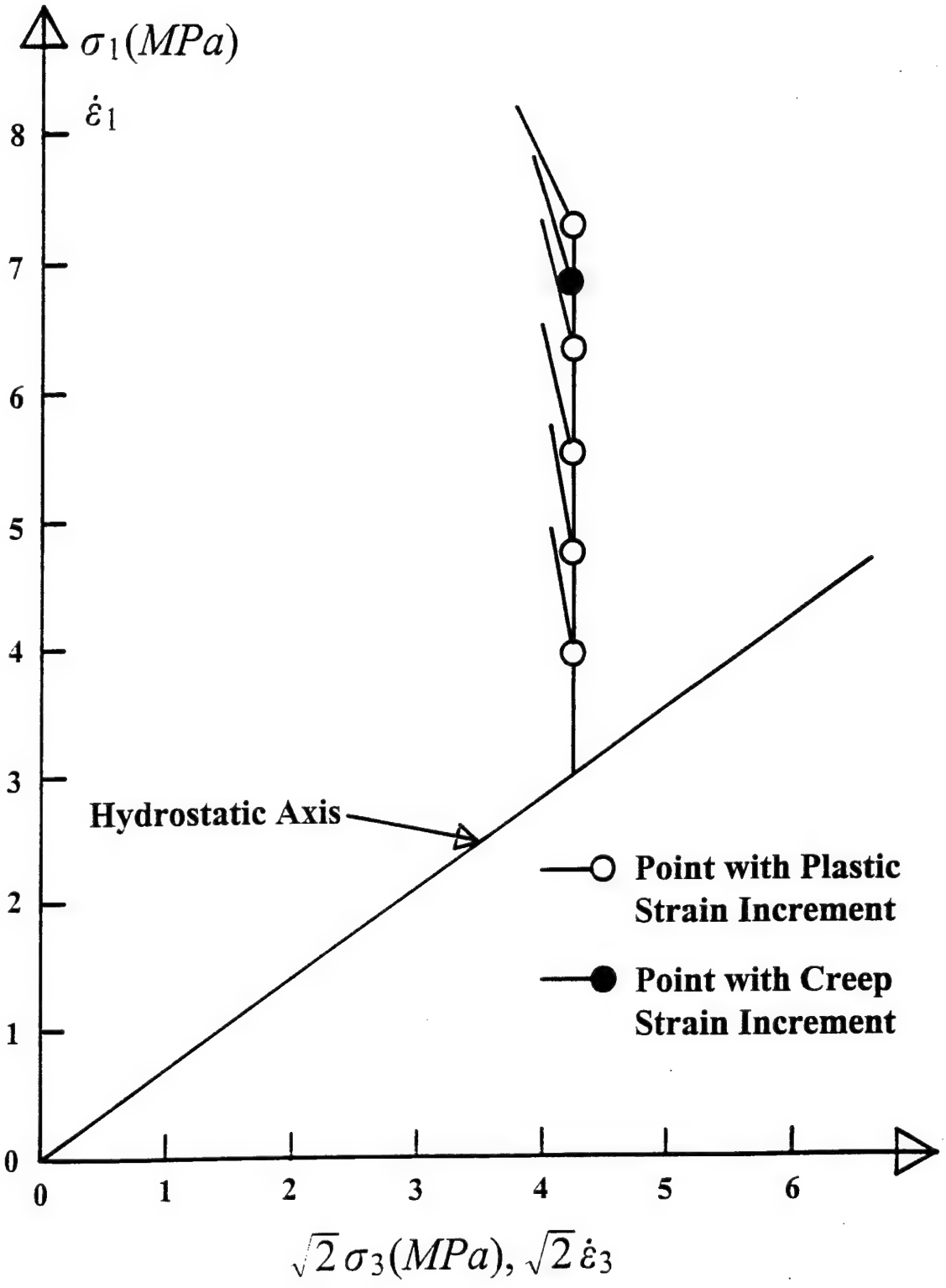

Fig. 12. Plastic and creep strain increment vectors superimposed on triaxial plane for triaxial tests performed to study instability of loose Sacramento River sand.

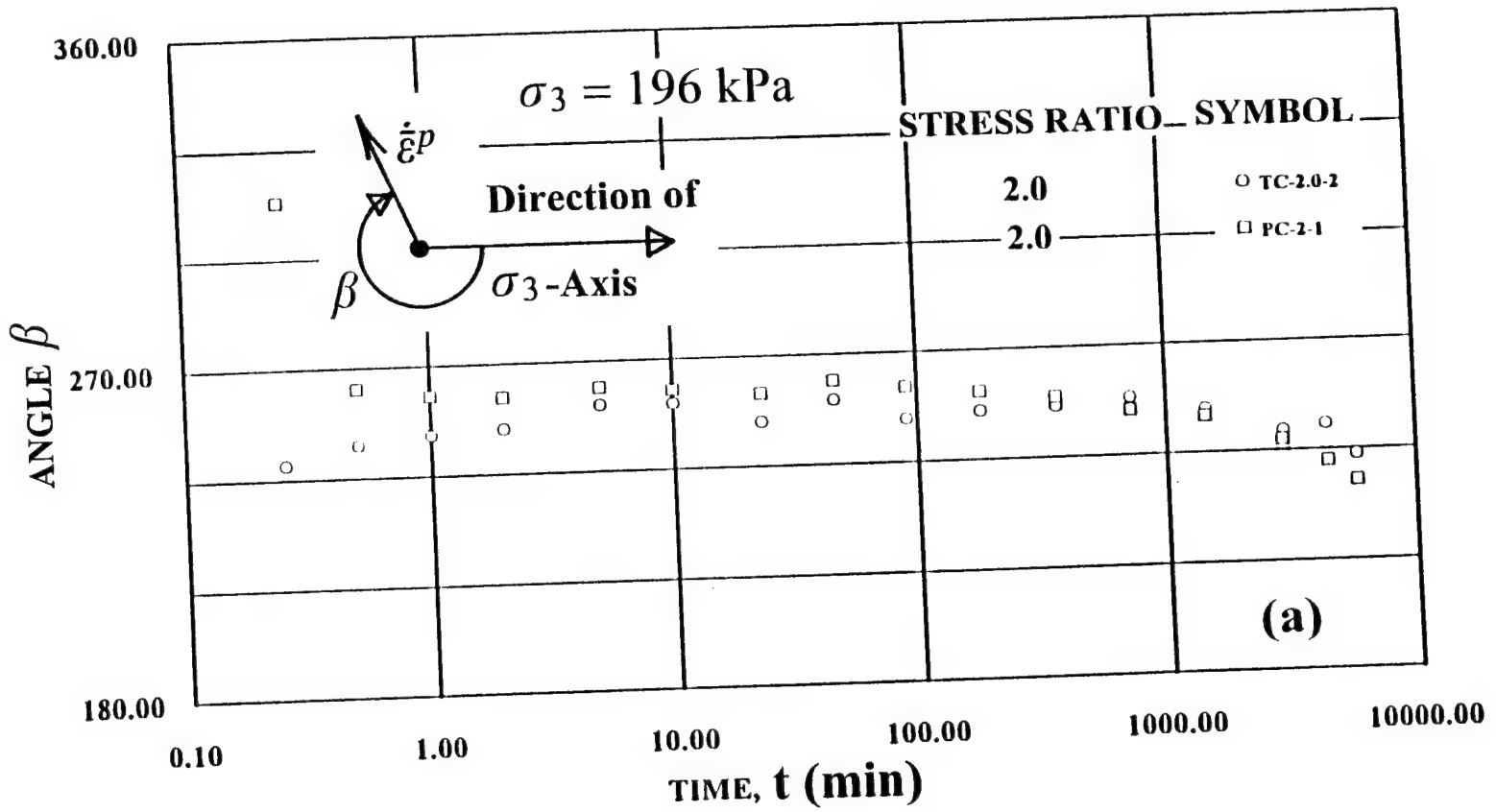

Fig.13. Variation of strain increment vector directions during creep with log(time) at (a) stress ratios = 2.0, and (b) stress ratios = 2.7 for Antelope Valley sand.

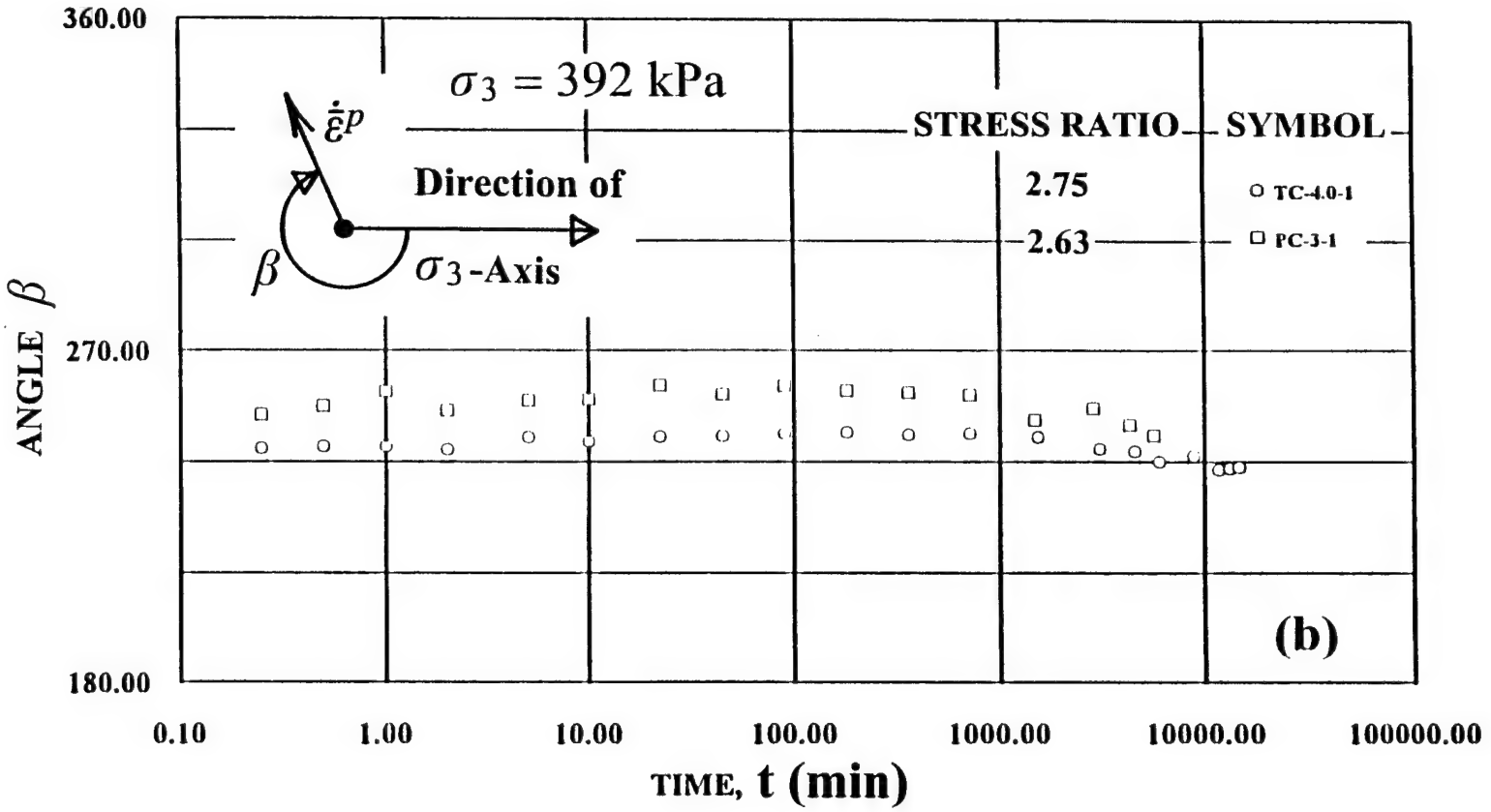

Fig.13.Variation of strain increment vector directions during creep with log(time) at (a) stress ratios = 2.0, and (b) stress ratios = 2.7 for Antelope Valley sand.

tendency towards compression of the sand. This is probably in response to crushing of grains, which may occur immediately following the stress change. Fracture of grains itself is a time effect, which then produces slight amounts of compression, because the smaller particles will fit better into the voids between the larger grains. A sieve analysis performed after one of the triaxial compression creep tests indicated approximately 20% passing the U.S. no. 200 sieve, where none of the sand passed this sieve before testing. However, as time passes, the yield surface is pushed out (see e.g. Lade 1994), and the diagrams in Fig. 13 show that the β angles decrease slightly, indicating that the sand becomes less contractive or more dilative again. This shows that the corresponding plastic potential surface moves out with the yield surface.

The time-independent plastic potential surface, defined as a surface that is perpendicular to the stain increments everywhere, is more curved at low stress ratios near the hydrostatic axis, and it becomes flatter or less curved at high stress ratios. In the flat region of the plastic potential surface, an increase in the stress difference will cause only small variations in the direction of the plastic strain increment vector. Therefore, creep effects on the direction of the inelastic strain increment vectors are smaller at higher stress ratios where larger amounts of creep occur.

In summary, it appears from these experiments that the yield surface and the plastic potential surface move out together, and the point at which to evaluate inelastic strain increment directions is at the current location of the yield surface and the accompanying plastic potential surface.

Mechanistic Picture

It may not be entirely unexpected that the same potential function applies to both creep and plastic behavior. Consider two grains which have just been sliding along one another, thus producing plastic deformation, as shown in Fig. 14. The creep deformation that follows the plastic deformation continues along the same contact direction, and the ratios between strains are therefore the same. It is quite reasonable to believe that an entire soil specimen, representing one element in the field, exhibits similar behavior as that pictured by the two grains. The ratios between creep strain increments are therefore logically the same as those for the plastic strain

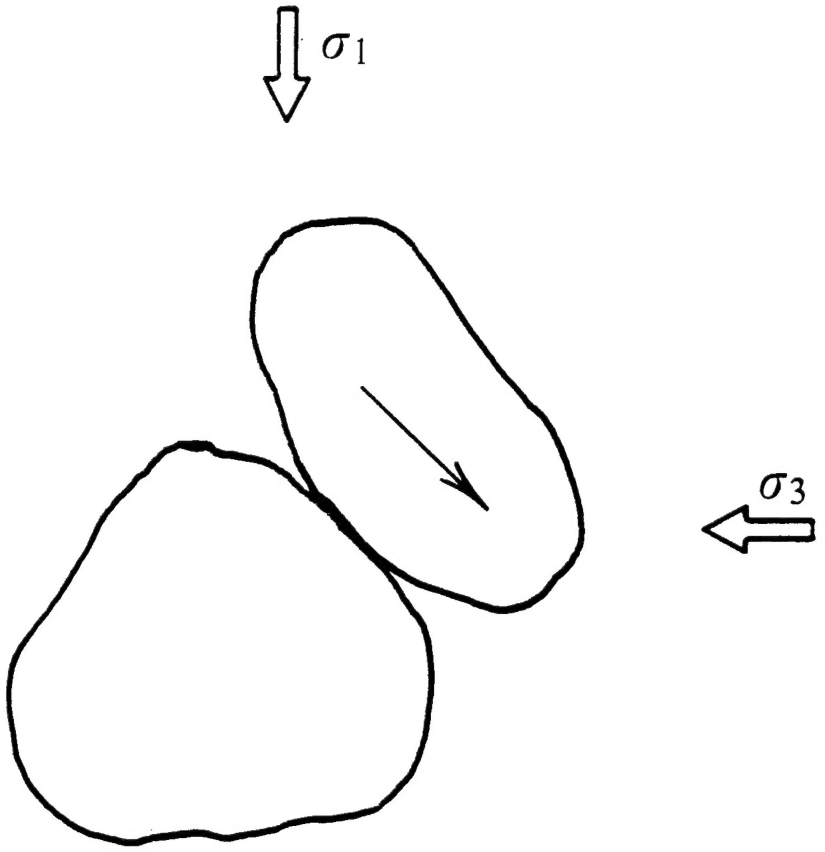

Fig. 14. Simple mechanistic picture of plastic sliding and creep along grain contact.

increment ratios. Consequently, the same potential function may be used to obtain both types of strain increments.

It may also be understood from this picture why the plastic potential should be evaluated at the current yield surface. Thus, if large creep strains occur, the particle fabric evolves, the yield surface is pushed out, and the state of stress required for further yielding changes. Since creep and plastic deformations both occur at grain contacts, as shown in Fig. 14, then the creep potential (= plastic potential) should be used at the stress state where further plastic deformation will occur, i.e. at the current yield surface.

CONCLUSION

An experimental study of drained creep in sand has been performed. This study was performed with attention to the factors that affect time-dependent deformations. Thus, the creep experiments were performed at constant temperature and constant confining pressure. Load control was used in the creep tests, while deformation control was employed in the constant strain rate tests. Techniques were developed to perform long term creep tests at several stages of each experiment. These included a method to avoid air and water leakage through the membrane into the triaxial specimen, and redundant methods of accurately measuring the linear and volumetric deformations.

Experiments were performed on a fine sand with sufficient permeability to observe creep deformations immediately following changes in stress. The nature of creep strains is similar to that of plastic strains in the sense that they may be predicted from the same framework provided by hardening plasticity theory. In particular, the potential surface determined from and used again for prediction of plastic strains may also be used for prediction of time-dependent creep strains. From the experiments it also appears that the yield surface and the plastic potential surface move out together, and the point at which to evaluate inelastic strain increment directions is at the current location of the yield surface and the accompanying plastic potential surface.

ACKNOWLEDGMENT

This research was sponsored by the Air Force Office of Scientific Research, USAF, under Grant Numbers 910117 and F49620-94-1-0032. Grateful appreciation is expressed for this support. The experimental work presented here was performed at University of California, Los Angeles.

APPENDIX. REFERENCES

Arulanandan, K., Shen, C.K., and Young, R.B. (1971). "Undrained creep behaviour of a coastal organic silty clay." *Geotechnique*, 21(4), 359-375.

Bishop, A.W. and Henkel, D.J. (1962) *"The measurement of soil properties in the triaxial test."* 2nd edition., Arnold, London.

Bjerrum, L. (1973). "Problems of soil mechanics and construction on soft clays and structurally unstable soils." *Proc. 8th Int. Conf. Soil Mech. Found. Engrg.*, 3, 111-159.

Bopp, P.A. and Lade, P.V. (1997). "Effects of initial density on soil instability at high pressures." *Journal of Geotechnical and Geoenvironmental Engineering,* ASCE, 123(7).

Chan, C.K. (1975). "Low-friction seal system." *Journal of the Geotechnical Engineering Division*, ASCE, 101(GT9), 991-995.

Chan, C.K. and Duncan, J.M. (1967). "A new device for measuring volume change and pressures in triaxial tests on soils." *Materials Research and Standards*, ASTM, 7(7), 312-314.

Feda, J. (1992). *"Creep of Soils and Related Phenomena."* Development in Geotechnical Engineering 68, Elsevier, Amsterdam.

Lade, P.V. (1994). "Creep effects on static and cyclic instability of granular soils." *Journal of Geotechnical Engineering*, ASCE, 120(2), 404-419.

Lade, P.V., Nelson, R.B., and Ito, Y.M. (1987). "Nonassociated flow and stability of granular materials." *Journal of Engineering Mechanics*, ASCE, 113(9), 1302-1318.

Lade, P.V., Nelson, R.B., and Ito, Y.M. (1988). "Instability of granular materials with nonassociated flow." *Journal of Engineering Mechanics*, ASCE, 114(12), 2173-2191.

Lade, P.V. and Pradel, D. (1989). "Comparison of single and double hardening constitutive models for frictional materials." *Proc. 3rd Int. Symp. Numerical Models in Geomechanics (NUMOG III)*, ed. by S. Pietruszczak and G.N. Pande, Elsevier Applied Science, London, 147-154.

Lee, K.L. and Vernese, F.J. (1978). "End restraint effects on cyclic triaxial strength of sands." *Journal of the Soil Mechanics and Foundations Division*, ASCE, 104(GT6), 705-719.

Leroueil, S. and Marques, M.E.S. (1996). "State of the Art: Importance of strain rate and temperature effects in geotechnical engineering." in *Measuring and Modeling Time Dependent Soil Behavior*, Geotechnical Special Publication No. 61, ASCE, ed. by T.C. Sheahan and V.N. Kaliakin, 1-60.

Mitchell, J.K. (1993). *"Fundamentals of Soil Behavior."* 2nd edition, John Wiley and Sons, New York.

Murayama, S., Michihiro, K. and Sakagami, T. (1984). Creep characteristics of sands." *Soils and Foundations*, 24(2), 1-15.

Tatsuoka, F. and Ishihara, K. (1974). "Yielding of sand in triaxial compression." *Soils and Foundations*, 14(2), 63-76.

Yamamuro, J.A. and Lade, P.V. (1993). "Effects of strain rate on instability of granular materials." *Geotechnical Testing Journal*, GTJODJ, ASTM, 16(3), 304-313.